HHS Public Access

Author manuscript

Dev Cell. Author manuscript; available in PMC 2024 October 23.

Published in final edited form as:

Dev Cell. 2023 October 23; 58(20): 2032–2047.e6. doi:10.1016/j.devcel.2023.07.020.

Skin type-dependent development of murine mechanosensory neurons

Charalampia Koutsioumpa[1], **Celine Santiago**[1], **Kiani Jacobs**[1], **Brendan P. Lehnert**[1], **Victor Barrera**[2], **John N. Hutchinson**[2], **Dhane Schmelyun**[1], **Jessica A. Lehoczky**[3], **David L. Paul**[1], **David D. Ginty**[1,*]

[1]Department of Neurobiology, Howard Hughes Medical Institute, Harvard Medical School, 220 Longwood Avenue, Boston, MA 02115, USA

[2]Bioinformatics Core, Department of Biostatistics, Harvard T.H. Chan School of Public Health, Boston, MA 02115, USA

[3]Department of Orthopedic Surgery, Brigham and Women's Hospital, Boston, MA 02115, USA

Summary

Mechanosensory neurons innervating the skin underlie our sense of touch. Fast-conducting, rapidly adapting mechanoreceptors innervating glabrous (non-hairy) skin form Meissner corpuscles, while in hairy skin, they associate with hair follicles, forming longitudinal lanceolate endings. How mechanoreceptors develop axonal endings appropriate for their skin targets is unknown. We report that mechanoreceptor morphologies across different skin regions are indistinguishable during early development but diverge postnatally, in parallel with skin maturation. Neurons terminating along the glabrous and hairy skin border exhibit hybrid morphologies, forming both Meissner corpuscles and lanceolate endings. Additionally, molecular profiles of neonatal glabrous and hairy skin-innervating neurons largely overlap. In mouse mutants with ectopic glabrous skin, mechanosensory neurons form end-organs appropriate for the altered skin type. Finally, *BMP5* and *BMP7* are enriched in glabrous skin, and signaling through type I BMP receptors in neurons is critical for Meissner corpuscle morphology. Thus, mechanoreceptor morphogenesis is flexibly instructed by target tissues.

Graphical Abstract

[*]Lead contact: david_ginty@hms.harvard.edu.

Author contributions

CK, CS, and DDG conceived the project and designed the experiments. CK performed and analyzed anatomical experiments with help from KJ and DS. CS and BPL performed DC/DCN injections. CK and CS performed the cell picking, single-cell sequencing, and analysis with help from VB and JH. VB and JH performed the reads alignment, QC, and integration analysis. CS performed DESEQ analysis. BPL and DLP provided advice throughout the course of this work. CK and DDG wrote the manuscript with input from all authors.

Declaration of interests

The authors declare no competing interests.

Inclusion and diversity

We support inclusive, diverse, and equitable conduct of research.

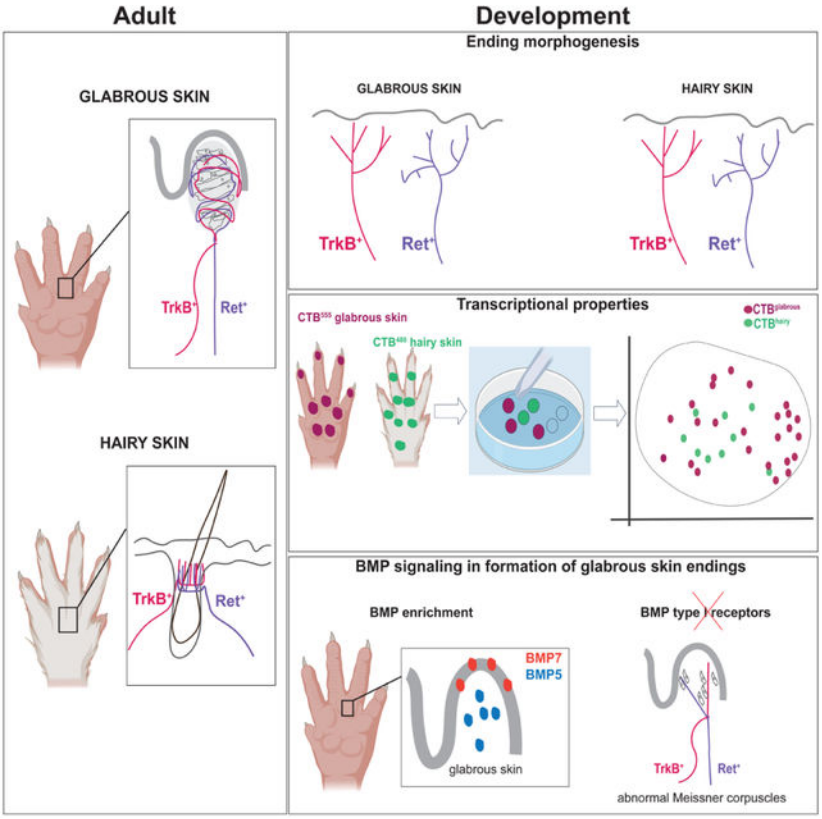

Koutsioumpa et al. characterize developmental steps leading to morphogenesis of mammalian tactile sensors innervating glabrous and hairy skin. They demonstrate that skin types differentially instruct sensory ending maturation, and signaling through neuronal BMP receptors is critical for the formation of Meissner corpuscles of glabrous skin.

Introduction

Our sense of touch allows us to identify and manipulate objects, communicate in social contexts, and detect and distinguish innocuous and harmful stimuli acting on the body. The first step leading to perception of, and reaction to, the heterogeneous repertoire of our tactile world is activation of touch sensory neurons, called mechanoreceptors, which have cell bodies residing in dorsal root ganglia (DRG) and trigeminal ganglia and form axonal endings in the skin.[1] The mechanoreceptors that detect light touch are the low-threshold mechanoreceptors (LTMRs). These neurons are morphologically and physiologically diverse, with subtypes responding to different mechanical stimuli, including gentle indentation of the skin, hair deflection, movement across the skin, and vibration.[2] Dysfunction of mechanoreceptors and their central circuits can lead to impaired sensation associated with neuropathies such as Charcot-Marie-Tooth disease, mechanical allodynia in neuropathic pain states, and hyperreactivity in certain developmental disorders.[3,4,5,6] Despite the critical importance of touch, the mechanisms of development and acquisition of morphological specializations of the cutaneous tactile sensors remain incompletely understood.[7]

Soon after neuronal commitment to different lineages, newborn DRG sensory neurons extend axons through a range of intermediate targets and into their final target tissues.[7] A key distinction between mechanosensory neurons arises from the skin target they innervate. In the mouse, glabrous (non-hairy) skin is localized to the ventral surface of the paws, whereas hairy skin is found across the body, including the trunk, tail, limbs, and dorsal surface of the paws. The cell bodies of hairy and glabrous-skin innervating LTMRs intermingle within limb-level (C5–C8 and L3–L5) DRGs[8] but their axonal specializations in the skin, called end-organs, differ according to the skin type they innervate. Present across mammalian species and sharing morphological and physiological properties,[9,10,11,12] the end-organs endow LTMR subtypes with the ability to extract salient features of external stimuli, including indentation, vibration, and movement across the skin.[1,13] Physiologically, LTMRs are classified based on their conduction velocity as Aβ, Aδ, and C, for rapid, intermediate, and slow conducting neurons, respectively, and according to their adaptation rate to skin indentation as rapidly adapting (RA), intermediate adapting (IA) or slowly adapting (SA).[2,14,15]

The different morphological features of glabrous and hairy skin LTMRs raise a fascinating and largely unexplored question: how is LTMR end-organ diversity achieved across different skin types? One possibility is that glabrous and hairy skin-innervating neurons are predetermined to form the distinct end-organs associated with the different skin types. Alternatively, the properties of LTMRs may be unspecified during early development, and glabrous and hairy skin may differentially instruct morphogenesis of their axon terminals, thus endowing them with characteristic end-organ structures and physiological response properties. The latter possibility is appealing because it would allow nascent mechanosensory neurons to flexibly acquire features relevant to the skin type they innervate.

Here, we sought to determine when and how the distinct morphological features of glabrous and hairy skin-innervating LTMRs arise over development, and begin to define molecular mechanisms underlying this process. We focused on Meissner corpuscle-innervating and lanceolate-ending forming LTMRs of glabrous skin and hairy skin, respectively, because, despite having common genetic labeling strategies in mice, their end-organ structures are strikingly distinct (Figure 1A, 1B, left panels).[16,17] In glabrous skin, Aβ LTMRs that express the neurotrophic factor receptors TrkB and Ret form Meissner corpuscles, which are end-organs nestled within dermal papillae. These Meissner corpuscle LTMRs detect light forces impinging on the skin as well as low-frequency vibrations.[18,19,20,21] On the other hand, in hairy skin, both Ret^+ Aβ RA-LTMRs and $TrkB^+$ Aδ-LTMRs form longitudinal lanceolate endings, which wrap around hair follicles, rendering them sensitive to hair deflection as well as indentation of the nearby skin.[17,19,22,23] Using anatomical, transcriptional, and mouse genetic approaches, we found that nascent Ret^+ and $TrkB^+$ mechanosensory neurons are not pre-determined to form a particular end-organ, rather these neurons can form either Meissner corpuscles or lanceolate endings depending on the skin type they innervate. Therefore, glabrous skin and hairy skin differentially instruct the morphological properties of nascent LTMRs. We also found that a glabrous skin-specific BMP type I receptor signaling pathway shapes the architecture of Meissner corpuscles but not hairy skin lanceolate endings. Our findings support a model in which skin type-specific

secreted cues instruct LTMR end-organ formation and thus their unique morphological and physiological response properties and functions.

Results

Distinguishing morphological features of glabrous skin- and hairy skin-innervating LTMRs arise postnatally

We first determined when fast-conducting, RA-LTMR axonal endings reach glabrous and hairy skin and acquire their specialized morphologies. To visualize sensory endings of developing Meissner corpuscle-innervating and lanceolate ending-forming LTMRs, we used *TrkB*^{GFP} or *TrkB*^{CreER}; *Avil*^{Flp}; *Rosa26*$^{LSL\text{-}FSF\text{-}tdTomato}$ mice[17,18] and prepared paw glabrous and hairy skin sections across a range of embryonic and postnatal ages. Immunochemistry for additional selected markers was also performed. At E15.5, labeled sensory neuron axons were observed in both glabrous and hairy skin. At this age, the axons expressed low levels of neurofilament (NFH, a marker of heavily myelinated DRG neurons) and had not yet localized to the epidermal-dermal junction. Moreover, at E15.5, S100^{+} Schwann cells, which in adulthood robustly associate with LTMR axons and are core cellular components of LTMR end-organs,[2] were present in low abundance (Figure 1A, 1B). By P5 in glabrous skin, nascent skin structures resembling dermal papillae and invaginations that give rise to eccrine sweat glands were observed;[24] specialized Schwann cells, termed lamellar cells, were found associated with LTMR axons and nascent corpuscles; and both sensory endings and lamellar cells began assuming the bulbous structure of the Meissner corpuscle. In hairy skin, a parallel process occurs around P5. Hair follicles with lanceolate ending structures encapsulated with S100^{+} Schwann cells – the terminal Schwann cells (TSCs)– were readily observed. By P50, both glabrous and hairy skin sensory end-organs had assumed their mature morphology (Figure 1A, 1B). These findings indicate that LTMR morphogenesis across skin types occurs in parallel with the development of skin appendages.

To investigate the development of more complex morphological features of LTMR endings, including axonal branching patterns, we used a sparse labeling genetic approach to view LTMR axons over different developmental timepoints. To study Meissner corpuscle-associated LTMRs in paw glabrous skin and lanceolate ending-associated LTMRs in paw hairy skin, we used mice with tamoxifen-inducible *TrkB*^{CreER} or *Ret*^{CreER} alleles combined with an alkaline phosphatase reporter *Brn3a*$^{f(AP)}$ allele.[25] We generated both *TrkB*^{CreER}; *Brn3a*$^{f(AP)}$ and *Ret*^{CreER}; *Brn3a*$^{f(AP)}$ mice from late-embryonic (E15.5) to young adult (P21) ages for collecting glabrous and hairy skin samples. The anatomical receptive fields and axonal branching patterns of TrkB^{+} and Ret^{+} neurons were then analyzed. Reconstructions of the axonal endings revealed that these LTMRs were present in both glabrous and hairy skin by E15.5, and exhibited similar “linear” terminal ending morphologies between E15.5 to P0 (Figure 1C, 1D, S1A, S1B, S2A–D). In contrast, at P5, nascent skin-type specific endings were evident, and these ending types continued to elaborate through P21, when more than 90% of the endings formed morphologically mature Meissner corpuscles and lanceolate endings in glabrous and hairy skin, respectively (Figure 1E). Additional morphological features of the labeled sensory neurons, including the number of branches per

neuron and the terminal ending area occupied, were also comparable in the two skin types at E15.5, however the neurons exhibited unique, skin type-specific features at P5 (Figure S1C, S1D, S1E, S1F). Our findings in paw hairy skin are in accordance with back hairy skin innervating LTMR development,[16] indicating that morphological properties arise similarly across hairy skin regions.

Thus, LTMR axonal morphogenesis takes place in distinct steps, with the initial appearance of simple axon terminals at late embryonic ages, followed by the formation of nascent Meissner corpuscle-like or lanceolate-like endings during the first postnatal week, and the near complete maturation of the end-organs during the second postnatal week. Additionally, the branching patterns, innervation area, and axonal ending properties of the labeled LTMRs are identical across glabrous and hairy skin types at E15.5, and by P5 they become highly distinct.

The presence of hairy skin/glabrous skin “border neurons” suggest that skin types instruct acquisition of LTMR morphological features

During the course of the sparse genetic labeling experiments using *TrkB*^{CreER}*; Brn3a*$^{f(AP)}$ and *Ret*^{CreER}*; Brn3a*$^{f(AP)}$ mice, we observed a small subset of neurons whose axons branch along the border of glabrous and hairy skin. Close inspection of these “border neuron” endings at P5 and P10 revealed that the same neuron can have branches that form both Meissner corpuscles in glabrous skin and lanceolate endings in hairy skin (Figure 2A, S3A and Supplementary Video 1–2). Furthermore, we found that these border neurons and their dual end-organ structures persisted into adulthood in both *TrkB*^{CreER}*; Brn3a*$^{f(AP)}$ and *Ret*^{CreER}*; Brn3a*$^{f(AP)}$ mice (Figure 2A–C, S3A and Supplementary Video 3). These findings raise the possibility that developing Ret^{+} and TrkB^{+} LTMRs have the capacity to become morphologically dissimilar Meissner corpuscle- or hair follicle lanceolate-ending forming LTMRs and that the skin region they innervate dictates their morphological properties.

We next asked whether border neurons are unique to Meissner corpuscles or lanceolate ending-associated LTMRs, or if they are observed across other sensory neuron types. The central projections of Aβ and Aδ-LTMRs exhibit dorsal horn branches and terminals, and many Aβ LTMRs exhibit an additional branch that ascends through the dorsal column (DC) and terminates in the dorsal column nuclei (DCN).[1] To randomly and sparsely label from a broad population of dorsal column-projecting Aβ LTMRs, we performed low-titer AAV-retro-Cre injections into the DCN or DC of *Brn3a*$^{f(AP)}$ mice (Figure 2D). In addition to the many labeled neurons found terminating in only glabrous or hairy skin, we once again observed several examples of border neurons, where branches of a single neuron extended across the glabrous/hairy border and formed endings appropriate for both skin types, Meissner corpuscles and lanceolate endings (Figure 2E). We also identified other morphologically distinct populations, including putative Aβ SA1-LTMRs that appeared to associate with specialized skin cells – Merkel cells– in both types of skin (Figure S3B). Therefore, border neurons are a feature of multiple LTMR subtypes, and a single LTMR can form morphologically distinct ending types in different skin regions.

Molecular profiling of glabrous and hairy skin innervating neurons

If neonatal paw-innervating TrkB$^+$ DRG neurons are able to become either Meissner corpuscle neurons or hair follicle lanceolate-ending neurons, then we may expect glabrous skin- and hairy skin-innervating TrkB$^+$ DRG neurons to be transcriptionally similar. The same would be expected for neonatal Ret$^+$ DRG neurons. To test this possibility, we sought to compare the transcriptomes of neonatal TrkB$^+$ and Ret$^+$ DRG neurons that innervate glabrous and hairy skin. However, published single-cell sequencing datasets of DRG neurons do not retain information about the skin targets innervated by the sequenced neurons. Therefore, we performed Smart-Seq of manually selected neurons innervating paw glabrous or hairy skin. For this, the retrograde tracer CTB^{488} was injected into dorsal/hairy forepaws and CTB^{555} was injected into ventral/glabrous forepaws and DRGs were collected at P5, a critical timepoint for LTMR end-organ formation (Figure S4A, S4B).

We targeted large diameter neurons for manual collection, because Aβ/Aδ LTMRs have large diameter cell bodies,[1] and collected 150 fluorescently labeled DRG neurons. Based on marker genes identified in previous studies,[26–28] the expression analysis revealed five clusters of sensory neurons (Figure 3A, S4C). We found that neonatal glabrous skin- and hairy skin-innervating Aβ/Aδ LTMRs did not segregate based on skin type innervation, but instead clustered together, and both the TrkB$^+$ and Ret$^+$ populations were transcriptionally distinct from other DRG neuron types (Figure 3A, 3B, S4C, S4D). These findings suggest that at least some glabrous and hairy skin-innervating sensory neuron populations have similar transcriptional profiles at P5, when acquiring their skin type-specific morphologies.

To place our glabrous skin-enriched dataset into a broader context and compare it with a larger population of hairy skin-innervating neurons, we integrated[29] our Smart-Seq dataset with a previously published P5 droplet-based single-cell dataset from DRGs across all axial levels (containing mostly sensory neurons innervating hairy skin) (Figure S4E).[27] By mapping the CTB-labeled paw-innervating neurons onto this larger dataset, we found that neurons clustered according to previously identified cell type markers[26–28] (e.g. *TrkA, TrkB, TrkC, Ret, Runx1, Runx3*) rather than by skin target (Figure 3C, 3D). In particular, TrkB$^+$ glabrous skin-innervating neurons were more similar to TrkB$^+$ neurons collected from all axial levels than to Ret$^+$ and other glabrous skin-innervating neurons. Likewise, Ret$^+$ glabrous skin-innervating neurons clustered together with other Ret$^+$ neurons collected from all axial levels and were distinct from other glabrous skin-innervating neurons. These results are consistent with our findings with the Smart-Seq dataset – at P5 neurons group by class rather than skin target. We further validated these findings by combining RNAscope *in situ* hybridization experiments using known markers of TrkB$^+$ and Ret$^+$ Aβ/Aδ LTMRs (*Ntng1*, *Colq*, and *Cadps2*). As with the scRNA-Seq findings, the RNAscope experiments showed that glabrous skin-innervating TrkB$^+$ and Ret$^+$ neurons express cell type-specific markers previously associated with TrkB$^+$ and Ret$^+$ neurons that innervate hairy skin (Figure 3E, 3F, 3G and 3H). Taken together, these findings suggest that the main axis by which DRG neurons transcriptionally vary during development corresponds to genetic identity and not the type of skin innervated.

The morphological properties of LTMRs are governed by the skin type they innervate

Our findings are consistent with the idea that neonatal TrkB$^+$ and Ret$^+$ neurons are competent to form either hair follicle lanceolate endings or Meissner corpuscles, and that the different skin types instruct the acquisition of their axon terminal morphology. To further test this idea, we generated genetically altered mice that have glabrous skin on both the ventral and dorsal sides of the paw and used them to examine whether this alteration affects the morphological properties of innervating LTMRs. We used *Prx1^{Cre}*; *Lmx1b$^{fl/fl}$* mice, in which the dorsal-limb specifying gene, *Lmx1b*,[30] is deleted in the limb mesenchyme.[31] *Prx1^{Cre}*; *Lmx1b$^{fl/fl}$* mice exhibit mostly glabrous skin on the dorsal surface of the paw with ectopic pedal pads in place of hairy skin (Figure 4A).[30] These resulting "double glabrous skin" mutant mice were used to assess whether sensory neurons that normally innervate hairy skin of the dorsal paw and form lanceolate endings around hair follicles, instead innervate ectopic glabrous skin of the dorsal paw and form Meissner corpuscles. While Meissner corpuscles were normally restricted to ventrally located glabrous skin of control mice, we observed large-diameter NFH$^+$ axons surrounded by S100$^+$ lamellar cells that formed Meissner corpuscles in both the ventral and dorsal surfaces of the paws in the double glabrous skin mutants (Figure 4B). The density and area of Meissner corpuscles in the ectopic glabrous skin (dorsal region of the paw) were comparable to those in the ventral glabrous skin of the mutants and control mice (Figure 4C, 4D). Importantly, the Meissner corpuscles observed in the ectopic glabrous skin were not formed by aberrant branching of ventrally projecting neurons: CTB injections with different fluorophores into the ventral glabrous skin and ectopic dorsal glabrous skin did not result in a statistically significant difference in the proportion of double-labeled DRG cell bodies compared to control mice (Figure S5D). Additionally, we visualized skin mRNA puncta of BDNF, which has been previously shown to be robustly expressed in the epidermis of glabrous skin, and found that it is expressed in the same pattern and levels between control glabrous and ectopic double glabrous mutant skin (Figure S5C).

We next asked whether TrkB$^+$ Aβ RA-LTMRs innervate the ectopic Meissner corpuscles by using Npy2r-GFP BAC transgenic mice, as previous findings showed that TrkB$^+$ Meissner afferents are labeled by the Npy2r-GFP transgene.[18] Thus, *Prx1^{Cre}*; *Lmx1b$^{fl/fl}$*; *Npy2r-GFP* mice were generated and used to immunolocalize GFP$^+$ axonal endings in the skin. Indeed, a large portion of ectopic Meissner corpuscles were innervated by two axons, one of which was GFP$^+$ (presumably TrkB$^+$) and one that was GFP$^-$ (presumably Ret$^+$), as previously observed in corpuscles of wild-type mice (Figure 4E).[18] The lamellar cell area associated with GFP$^+$ endings in Meissner corpuscles of double glabrous mutants was smaller than those of control mice, possibly reflecting a difference in their location (Figure S5A). Nevertheless, these findings indicate that many ectopic Meissner corpuscles of the double glabrous mutant mice were dually innervated, as observed in Meissner corpuscles of wildtype mice.

Other sensory neuron ending types, including NFH$^+$ axons associated with epidermal Merkel cells (Troma$^+$), which are putative Aβ SA1-LTMRs, were also present in the ectopic skin of double glabrous skin mutants (Figure S5B). In forelimb level DRGs, quantification of NFH$^+$ neurons and IB4$^+$ small diameter neurons revealed no differences between controls

and mutants (Figure S5E, S5F). Moreover, no obvious differences were observed in the spinal cord dorsal horn by synaptic marker expression[32] (Figure S5G). Finally, *TrkB*$^{+}$ sensory neurons innervating the ectopic glabrous skin of double glabrous skin mutant mice also expressed Aβ/Aδ LTMR markers, including *Ntng1* and *Colq* (Figure S5H). Overall, these observations indicate that morphogenesis of the cutaneous endings of TrkB^{+} and Ret^{+} LTMRs is dictated by the skin region that these neurons innervate.

BMP signaling differentially influences glabrous ending morphogenesis

Our findings that the skin region instructs the acquisition of LTMR morphological features led us to consider whether skin region-derived cues are critical in this process. Murine and human skin develop into glabrous or hairy under the tight control of morphogens that originate from the associated mesenchyme; a bone morphogenetic protein (BMP) signaling pathway is instructive for glabrous skin-specific appendage development, whereas sonic hedgehog (SHH) and a SHH: BMP imbalance promotes hair follicle morphogenesis.[24] Therefore, we hypothesized that morphogenic factors that govern glabrous and hairy skin development also shape the terminal structures of resident LTMRs. Indeed, BMPs, which act through BMP type I and type II receptors and control tissue patterning throughout the body[33], are expressed in the skin during development.[24,34,35,36,37] Moreover, qPCR experiments showed that *BMP5* and *BMP7* are selectively enriched in glabrous skin[24] rendering them poised to act on sensory neurons innervating this skin type. Additionally, the BMP canonical pathway and transcriptional modulators of BMP signaling are developmentally regulated in DRG neurons.[38] However, whether BMP signaling influences skin type-specific end-organ development is unknown.

To examine the developmental dynamics of BMP expression in glabrous and hairy paw skin, we used *in situ* hybridization (RNAscope) to localize mRNA transcripts of different members of the BMP ligand family. At P5, we found that *BMP4* and *BMP7* were present in both glabrous and hairy skin, while *BMP5* was selectively enriched in glabrous skin (Figure 5A, top panels). Quantifications of puncta density revealed that BMP4 is expressed both in glabrous and hairy skin, BMP5 was only detectable in glabrous skin, and BMP7 was highly enriched in glabrous skin (Figure 5A, bottom panels). On the other hand, a BMP antagonist, *Grem2*, was present in hairy skin but absent from glabrous skin (Figure 5A). We next assessed the developmental dynamics of *BMP5* expression in the skin, as it was selectively located in glabrous skin at P5, a critical time point for LTMR morphogenesis (Figure 1). In E17.5 skin, when nascent sensory neurons are present in the skin dermis and still morphologically undifferentiated (Figure 1), *BMP5* mRNA was highly expressed and spatially restricted to glabrous skin dermis while virtually absent in hairy skin (Figure 5B). This differential expression pattern persisted through adult ages (Figure 5B). Interestingly, *BMP5* was not expressed homogeneously across the glabrous skin dermis. Rather, *BMP5* transcripts were enriched in the dermis of nascent fingertips and pedal pads, where Meissner corpuscles are found, and in low abundance or absent in glabrous skin regions between the pads, which are not populated by Meissner corpuscles (Figure S6A, S6B). Thus, *BMP5* is highly expressed and spatially restricted to the precise locations where Meissner corpuscles develop. Additionally, we examined whether it is present in the ectopic glabrous skin of the double glabrous mutants, which is populated by Meissner corpuscles (Figure 4C), and

found that BMP5 was present in a comparable density compared to control glabrous skin (Figure S6C). We, therefore, hypothesized that BMP signals emanating from the skin act through BMP receptors in sensory neurons to specify morphological properties of glabrous skin-innervating LTMRs.

To test this possibility, we next examined the integrated sensory neuron transcriptomic dataset to determine whether certain BMP type I receptors are present in sensory neurons innervating the skin. Indeed, *Bmpr1a* and *Acvr1* were expressed across multiple LTMR populations in development, while *Bmpr1b* expression was restricted to subsets of developing CGRP$^+$ neurons (Figure S7A). To selectively ablate BMP signaling through BMP type I receptors, we generated *Avil^{Cre}; Bmpr1a$^{fl/fl}$; Acvr1$^{fl/+}$* and *Avil^{Cre}; Bmpr1a$^{fl/fl}$* mice, which have the *Bmpr1a* and/or *Acvr1* receptor genes deleted in all somatosensory neurons beginning ~E12.5,[39] and compared them to their littermate controls. General skin features appeared normal in the mutants, with dermal papillae and sweat glands both present (Figure 6A). However, adult mutant mice demonstrated a decrease in Meissner corpuscle density, 0.29 corpuscles per dermal papilla in mutant mice compared to 0.40 Meissner corpuscles per dermal papilla of control mice (Figure 6A, 6B). Most strikingly, we observed that the structure of Meissner corpuscles was highly abnormal in the mutants. Normally, Meissner corpuscles are comprised of LTMR axon terminals, four or more lamellar cells that wrap around the axons, and one or more capsule cells, located within dermal papilla, closely surrounded by epithelial cells.[40,41] A hallmark of Meissner corpuscles is the lamellar cell core, which defines the globular morphology of the corpuscle and is considered critical for its function.[2] In mutant mice, the S100$^+$ lamellar cells were highly disorganized and occupied a small area in both the fingertips (81 μm^2 in mutant mice compared to 205 μm^2 in control mice) and pedal pads (84 μm^2 in mutants and 246 μm^2 in controls) of glabrous skin (Figure 6C, 6D). In addition, quantifications of the nuclei of S100$^+$ glial cells in dermal papillae and in the lamellar core demonstrated decreased numbers in the mutant tissue (Figure S7B).

We also examined LTMR endings in hairy skin, where we had observed expression of certain BMPs, specifically *BMP4* and *BMP7* (Figure 5A). We quantified the S100 area of the longitudinal lanceolate endings (Figure 6E, 6G), which in paw hairy skin are formed by TrkB$^+$ and Ret$^+$ LTMRs and in back hairy skin by TrkB$^+$ and Ret$^+$ LTMRs and C-LTMRs. Both the S100 area and the number of TSCs were similar in control and mutant paws and back hairy skin (Figure 6F, 6H). Therefore, hairy skin innervation by lanceolate ending-containing LTMRs appeared normal. We also used synaptic markers to examine dorsal horn synaptic architecture[32] of the mutant mice and no differences were observed (Figure S7C). In addition, mutants and controls had similar numbers of NFH$^+$ and IB4$^+$ neurons in limb-innervating cervical (C5–C8) DRGs (Figure S7D).

The findings that certain BMPs are highly enriched in glabrous skin during the period of LTMR skin innervation, and that BMP type I receptors are required in sensory neurons for formation of Meissner corpuscles, but not hair follicle lanceolate endings, support a model in which BMPBMPR signaling instructs glabrous skin-innervating LTMRs to form Meissner corpuscles.

Discussion

Little is known about the steps leading to LTMR development across different skin types. Here, we used anatomical, transcriptional, and mouse genetic approaches to describe the timing of murine mechanosensory neuron development and the role of skin targets in instructing LTMR end-organ maturation. We investigated hairy skin and glabrous skin LTMR subtypes that are labeled by TrkB and Ret genetic tools because the labeled neurons exhibit distinct features depending on the skin type they innervate; Meissner corpuscles in glabrous skin and longitudinal lanceolate endings surrounding hair follicles in hairy skin. Our findings support a model in which, during early stages of development at the onset of skin innervation, nascent $TrkB^+$ and Ret^+ LTMRs have the capacity to form different end-organs, and their distinct morphological properties are instructed by signals originating from the skin type they innervate (Figure 7).

Skin-type dependent LTMR morphological maturation and molecular profiles of glabrous and hairy skin innervating neurons

Previous work in other sensory systems has demonstrated that the pairing of intrinsic and extrinsic cues leads to neuronal diversity.[42] In the auditory system, for example, spiral ganglion neurons undergo a gradual emergence of identity during postnatal development and acquire their mature properties through a combination of intrinsic and extrinsic signals, including inner hair cell activity.[43] We characterized the stepwise morphological development of glabrous and hairy skin-innervating LTMRs, which arise in parallel with the maturation of the skin niche. We found that nascent $TrkB^+$ and Ret^+ LTMRs can form either Meissner corpuscles or lanceolate endings and that the skin target region they encounter differentially instructs their morphological maturation. Thus, we propose that hairy and glabrous skin-innervating neurons encounter distinct sets of skin-derived cues that instruct their respective morphological properties and interactions with other cell types, including terminal Schwann cells and lamellar cells. This enables remarkable flexibility in the developing mechanosensory system and the capacity to adapt to changing and evolving environmental needs.

Using single-cell transcriptomics of developing glabrous skin- and hairy skin-innervating neurons we found that cells segregate by previously known transcriptionally defined classes independently of the skin type they innervate. We used a retrograde labeling strategy to enrich forepaw-innervating neurons for our transcriptomic analysis. This strategy, paired with deep sequencing allowed for sufficient granularity to reveal molecular signatures of glabrous skin-innervating neurons. As such, the present study adds an additional dimension –that of skin target region– to complement currently available DRG transcriptomic datasets.[26,27] Our findings do not exclude the possibility of transcriptional differences between hairy and glabrous skin-innervating neurons. Indeed, we performed a pseudo bulk sequencing analysis (see Methods) and identified a small number of genes enriched in either hairy skin- or glabrous skin-innervating neurons (Supplementary Table 1).

BMP signaling and the maturation of Meissner corpuscles

Developing somatosensory neurons encounter extrinsic cues that promote their maturation, survival, axon extension, target innervation, and ending formation.[7] Indeed, a range of trophic and tropic cues, extracellular matrix and cell membrane-bound cues, and physical forces act on developing somatosensory neuron subtypes.[7] Among the skin-derived cues that instruct mechanosensory neuron axonal features is the neurotrophin BDNF, which is essential for Meissner corpuscle development, Aδ-LTMR lanceolate ending polarization around hair follicles, and axonal branching in nascent mammary gland.[17,18,44]

Our findings point to a key role for skin-derived BMP ligands in Meissner corpuscle morphology. In related work, BMP4 was found to promote Merkel cell clustering around guard hairs,[45] and inhibition of BMP signaling in the skin through noggin overexpression in keratinocytes led to an increased density of cutaneous sensory endings.[46] In trigeminal neurons, a convergence of neurotrophin and BMP retrograde signals promotes neuronal transcriptional identity and central axon targeting.[47,48,49] Whether in these contexts, BMPs act locally or long-range to exert their effects is not known. The finding that BMP signaling is required for the morphological properties of glabrous skin-innervating $TrkB^+$ and Ret^+ LTMRs, which form Meissner corpuscles, but not their hairy skin counterparts that form lanceolate endings around hair follicles, supports the view that BMPs have unique functions across different skin types. Possible explanations include an imbalance in total BMP levels in the two skin types, critical roles of specific members of the BMP family (e.g. *BMP5* or *BMP7*) that are temporally or spatially enriched in glabrous skin and the presence of BMP antagonist(s) localized in hairy skin. Future work will be needed to determine whether abnormal Meissner corpuscle formation in mice lacking neuronal BMP signaling is caused by disorganized migration or failure of maturation of the lamellar cells within dermal papilla or some other step in the genesis of mature corpuscles. As an alteration in BMP signaling impairs both Meissner corpuscle axons and lamellar cells, it is possible that dysfunction of one cell type disrupts the other. On one hand, neuronal projections arrive in the skin prior to glia cell migration into dermal papillae, and one possibility is that some aspect of early axonal extension into dermal papillae is altered in the absence of BMP signaling. It is also possible that lamellar cells are dysfunctional and this leads to altered corpuscle morphology because these cells play a key role in maintenance of cutaneous axonal endings.[23] Finally, while our findings implicate BMP signaling in Meissner corpuscle formation, future studies should explore the roles of signals emanating from hairy skin, perhaps SHH and WNTs,[24,34] in instructing morphogenesis of hair follicle-associated endings.

In sum, our findings help to delineate how somatosensory neurons acquire their unique morphological properties across different regions of the body and point to a remarkable developmental flexibility in their capacity to form distinct end-organ structures in a skin-type dependent manner. These findings may aid in the quest to understand how disruption of DRG sensory neuron development and function can lead to clinical pathologies affecting somatosensation. It is also noteworthy that BMP signaling has been implicated in DRG regenerative transcriptional responses.[50] Therefore, target-derived cues that act during development to specify skin type-specific morphological properties may also contribute to

regeneration of the cutaneous end-organs of touch following their loss because of skin injury or disease.

Limitations of the study

Here, we investigated how mechanosensory neurons acquire their unique morphological features, which ultimately underlie their physiological properties and roles in tactile sensing. While we have focused on large-diameter sensory neurons (mainly Aβs/Aδ subtypes), future work will be needed to capture properties of small-diameter DRG neurons that innervate glabrous skin and identify cues that control their maturation. Additionally, we studied the role of BMP type I receptors on Meissner corpuscle formation, however, due to limited litter sizes and lethality, the contributions of individual BMP type I receptor alleles were not fully explored. Finally, further work is needed to address the roles of different BMP ligands in Meissner corpuscle formation.

STAR Methods

Resource availability

Lead contact—Further information and requests for resources and reagents should be directed to and will be fulfilled by the lead contact, David Ginty (david_ginty@hms.harvard.edu).

Materials availability—Single-cell Smart-Seq data are deposited at Dataverse (https://doi.org/10.7910/DVN/WA4OU1) and GEO (GSE229111).

Data and code availability

- Single-cell RNA-seq data have been deposited at GEO and Dataverse and will be publicly available. Accession numbers are listed under the Materials availability Methods section. Microscopy data reported in this paper will be shared by the lead contact upon request.
- This paper does not report original code. The scripts used are available and will be shared by the lead contact upon request.
- Any additional information required to reanalyze the data reported in this paper is available from the lead contact upon request.

Experimental model and study participant details—All mouse handling and procedures were performed according to animal protocols approved by the Harvard Medical School Institutional Animal Care and Use Committee (IACUC). Animals were group housed (1–5 mice per cage) according to gender, in a temperature- and humidity-controlled facility and were maintained on a 12-h light/dark cycle. For cell isolation, single cell sequencing and RNAscope validation experiments, wildtype CD1 mice were used. For all other experiments, the mouse lines were maintained on a mixed background.

Mouse lines—The mouse lines used include: *Avil*^{Cre} (JAX 032536), *Ret*^{CreER} (MGI 4437245), *TrkB*^{CreER} (JAX 027214), *Prx1*^{Cre} (JAX 005584), *Advillin*^{Flp} ,

Rosa$^{LSL\text{-}FSF\text{-}Tdtomato}$ (Ai65) (JAX 021875), *Brn3a*$^{f(AP)}$ (JAX 010558) *Npy2r-GFP* (MGI 3844094), *TrkB*^{GFP}(JAX 023046) , *Lmx1b*^{fl} (JAX 031287), *Bmpr1a*^{fl}, and *Acvr1*^{fl} mice.[17,18,19,25,39,52,53,54] E15.5 – P50 male and female mice were used for histological experiments. For sequencing analysis and DRG RNAscope P4–P6 wild type mice were used (CD1 mice, strain #022 from Charles River). For skin RNAscope the tissue and analysis were performed on wild type E17.5 – P30. DRG and spinal cord anatomy was performed on mice collected from P16-P35. At least three animals per genotype were tested for each experiment, unless otherwise noted in the figure legends. The morning that a vaginal plug was observed after mating setup was counted as E0.5.

Tamoxifen treatment—Tamoxifen (Sigma) was dissolved in ethanol (20 mg/ml) and an equal volume of sunflower seed oil (Sigma) was added. Following vortexing for approximately 15 minutes, the mixture was centrifuged under vacuum for 60 minutes to evaporate ethanol. The stock solution was kept at −80°C and warmed up to room temperature before administration. Pregnant females were treated with oral gavage (E11.5 for *Ret*^{CreER}, E12.5/E13.5/E14.5 for *TrkB*^{CreER}). 0.8–1mg were used for sparse labeling and 3mg were used for dense labeling.

Method details

Tissue collection and fixation for immunohistochemistry—Animals P6 or younger were first anesthetized using ice and decapitated. Mice that were older than P7, were anesthetized using isoflurane and were subsequently transcardially perfused using ~15ml ice cold 1x Phosphate Buffered Saline (PBS) and ~15ml 4% Paraformaldehyde (PFA) prepared in 1x PBS. Paw or back hair were removed using commercial hair removal cream Nair (Church and Dwight Co.; Princeton, NJ) for 3 minutes. Post fixation was performed in Zamboni fixative (Fisher # NC9335034) for skin and 4% PFA for spinal cord and DRGs at 4°C, overnight. 1x PBS was used the day after for washing off the fixative (2 to 3 10-minute washes). For skin that was prepared for GFP immunostaining, a lighter fixation protocol was used; after anesthetization, skin pieces were collected and drop-fixed in 1% PFA in 1x PBS for 2 hours at 4°C. 1x PBS was used for washing off the fixative. Tissues were stored in 1x PBS at 4°C.

Cryo-sectioning and immunohistochemistry—For cryo-sectioning, the tissues were dissected and cryoprotected in 20–30% sucrose at 4°C overnight. The next day the tissue was embedded in OCT (Fisher #1437365) or Neg50 (Fisher #7732-18-5) over dry ice in 100% ethanol and frozen tissues blocks were transferred to −80°C for storage. Before cryo-sectioning, the frozen tissue blocks were transferred inside the −20°C cryostat and allowed to equilibrate for 30 minutes before sectioning. Spinal cord and DRGs were sectioned at 20 μm while skin was sectioned at 25 μm. For the density measurements, 1 out of 3 consecutive sections was added on the slide to avoid double-counting of the neurons. Following that, the slides were left to dry overnight at room temperature before proceeding for immunohistochemistry. For slides that were not immediately stained, storage at −20°C was performed.

For immunohistochemistry, a PAP pen (Vector laboratories #H-4000) was used to create a hydrophobic barrier around the sections. The slides were washed once for 5 minutes with 1x PBS and 3 times for 10 minutes with 0.1% Triton X-100 in 1x PBS (0.1% PBST). A blocking step (5 % normal donkey or normal goat serum in 0.1% PBST) of 1 hour at room temperature was followed by the addition of the primary antibody mixture, prepared in the blocking solution. After 1 −2 days of 4°C incubation, the slides were washed 3 times for 10 minutes with 0.1% PBST. Secondary antibodies prepared in the blocking mix were added and slides were left at 4°C overnight. The next day, the slides were washed, mounted and coverslipped with DAPI Fluoromount-G (Fisher #0100–20), and imaged or stored in a slide box at 4°C.

For wholemount immunohistochemistry, back hairy or paw hairy skin were collected and fat tissues were peeled off using a stainless-steel spatula. The skin was fixed in Zamboni fixative (Fisher # NC9335034) overnight at 4°C. The next day, tissues were rinsed 3 times for 10 minutes at 1x PBS and then washed with PBS containing 0.3% Triton X-100 (0.3% PBST) every 30 minutes for a total of 6 hours. Following that, a primary antibody mixture prepared in blocking solution (0.3% PBST containing 5% goat or donkey serum and 20% DMSO) was added and incubated at room temperature for 4–5 days. Then, the tissues were washed in 0.3% PBST every 30 minutes for a total of 6 hours. The secondary antibody mix prepared in blocking solution was then added and allowed to incubate at room temperature for 3 to 4 days. Then, the tissues were washed in 0.3% PBST every 30 minutes for a total of 6 hours and dehydrated in 50% methanol for 15 min, 80% methanol for 15 min, and 100% methanol overnight. Then, the tissues were cleared in BABB (Benzyl Alcohol, Sigma #402834; Benzyl Benzoate, Sigma #B-6630; 1:2) at room temperature for 10 min and imaged.

The following dilutions and primary antibodies and lectins were prepared : chicken polyclonal anti-NFH (Aves # NFH0211, 1:500), rabbit anti-NF200 (Sigma # N4142, 1:500), mouse monoclonal anti-NeuN (Millipore # AB_2298772, 1:500), rabbit polyclonal anti-S100 Beta (Fisher #15146–1-AP, 1:500), rat polyclonal anti-Troma1 (DSHB #AB_531826, 1:50), rabbit anti-DsRed (Clontech #AB_10013483, 1:500), goat anti-GFP (Abcam #AB_305635, 1:500), goat anti-mCherry (CedarLane # AB0040–200, 1:500), guinea pig anti-vGluT1 (Millipore #AB_2301751; 1:1000), rabbit anti-Homer1 (Synaptic Systems #160003, 1:1000), Isolectin B4 647 (Invitrogen #SCR_014365, 1:500). The secondary antibodies used were Alexa 488, 546 or 647 conjugated donkey or goat anti-mouse, rabbit, chicken, goat or guinea pig (Life Technologies or Jackson ImmunoResearch) and were prepared at 1:500 dilution.

Whole-mount alkaline phosphatase staining—For sparse labeling experiments *Ret*^{CreER}*; Brn3a*$^{f(AP)}$ and *TrkB*^{CreER}*; Brn3a*$^{f(AP)}$ mice were used. Whole-mount placental alkaline phosphatase staining was performed following previously published protocols.[8] In brief, E15.5, P0, P5, P10, P21 and P50 mice were euthanized as described in the tissue collection section above. Following overnight fixation in Zamboni fixative at 4°C and PBS washes on the next day, the forepaw and hindpaw glabrous and hairy skin were dissected. The skin was placed in Eppendorf tubes in 1x PBS and incubated at 65 °C for 2 hours. The tissues were then washed with B3 buffer (0.1 M Tris pH 9.5, 0.1 M NaCl, 50 mM

MgCl2) 3 times for 15 minutes at room temperature. Subsequently, they were incubated in BCIP (Sigma #11383221001)/NBT (Sigma # 11383213001) buffer (3.4 μl/ml each) in B3 buffer with 0.1% Tween-20 overnight at room temperature. The next day, tissues were washed with 1x PBS and fixed with 4% PFA/PBS for 1 hour at room temperature. Following rinsing with 1x PBS, tissues were dehydrated sequentially for one hour each with 50%, 75%, and overnight 100% ethanol. They were then cleared in BABB before imaging. The same protocol was also followed for P14 and P50 *Brn3a*$^{f(AP)}$ mice that had Cre injections in the Dorsal column. The Simple Neurite Tracer plugin at Fiji (https://imagej.net/plugins/snt/) was used to trace the axonal skin endings. The axons were aligned across the image stack using the Linear Stack Alignment Registration plugin at Fiji.

Cre virus injections into dorsal column (DC)/dorsal column nuclei (DCN)—The injections were performed as previously described. Mice were placed on a stereotactic surgery frame, and their dorsal column was exposed at C1–C2 levels. Dorsal column injections of 100–200 nL of rAAV2/1-Cre virus (Penn Viral Core, diluted to 2E12 vg/mL) were performed at approximately 200 microns below the spinal cord surface. Following the injection, the mouse skin was sutured and mice were placed in a warm recovery box before being returned to their cage for postoperative monitoring.

Tissue collection and processing for RNAscope—P4–P6 animals were anesthetized in ice for 2–4 minutes or until unconscious, then sacrificed quickly by decapitation. P7 and older mice were first euthanized by CO_2 and then decapitated. The tissue - glabrous skin/paw hairy skin/spinal cord level C5–C8 DRGs/ thoracic or C2–C3 DRGs - was exposed accordingly and rapidly dissected. The tissues were placed on a cast on cold OCT and then frozen in dry ice-cooled 2-methyl butane for 3 minutes. The frozen blocks were stored at −80 °C. The tissue was subsequently placed inside the −20 °C cryostat for 30 minutes to 1 hour and then sectioned 18–20 μm for skin and 20 μm for DRGs. The slides with the sections were left at the cryostat for 1 hour and then stored at −80 °C.

RNAscope—Skin tissues were postfixed for 1 hour at 4°C and the RNAscope v.2 was performed according to the manufacturer's protocols for fresh frozen tissue (Acdbio #323110, # 322381). DRGs were postfixed for 15 minutes at 4°C. The DRGs from CTB-injected skin were postfixed in 10% Neutral buffered saline (NBF) (Sigma #HT5012–1CS) for 1 hour at room temperature. RNAscope was performed according to the manufacturer's protocols RNAscope v.1 for fresh frozen tissue (Acdbio #320851, 322340). the slides were mounted and coverslipped with DAPI Fluoromount-G (Fisher Cat #0100–20) and imaged or stored in a slide box at 4°C.

The following probes were used: Mm-Ntng1-C1 and C2 (Acdbio #488871, 488871-C2), Mm-Cadps2-C2 (Acdbio #529361-C2), Mm-Ret-C3 (Acdbio #431791-C3), Mm-Ntrk2-C3 (Acdbio # 423611-C3), Mm-Colq-C2 (Acdbio #496211-C2), Mm-Bmpr1a (Acdbio #312421), Mm-Krt14 (Acdbio #422521), Mm-Bmp7 (Acdbio #407901), Mm-Bmp4-C3 (Acdbio #401301-C3), Mm-Bmp5 (Acdbio #401241), Mm-Grem1-C2 (Acdbio #314741-C2), Mm-BDNF (Acdbio #424821), Probe diluent (Acdbio #300041). For the RNAscope v.2 kit, the following Opal dyes were used: Opal 570 (Akoya # FP1488001KT), Opal 690 (Akoya # FP1497001KT), and Opal 520 (Akoya # FP1487001KT). For quantification of the

density of puncta in the skin, we used a custom script in Fiji, creating a mask for puncta, and thresholding for *BMP4/BMP5/BMP7/Grem2* using the same threshold for all conditions. Puncta were quantified and the resulting puncta number was divided by the image area to produce the density estimates.

Skin CTB injections—Mice P3–P4 were anesthetized using ice for 2 to 3 minutes. CTB^{647} (Cholera Toxin Subunit B 647 Conjugate, Fisher # C-34778) was prepared in 1x PBS to a final concentration of 50–100mg/ml and mixed with a small amount of fast green (Sigma #F7252–5G). Injections were done using a fired polished and beveled glass pipette (Drummond #50002005). The glabrous or hairy skin were first cleaned using 1x PBS, then the dermal locations of interest were injected (middle of the paw hairy skin, pedal pads, and fingertips of the glabrous skin). 0.5–1 μL of CTB was injected per spot. Following the injection, the mice were placed on a warming pad and left to recover before placing them in their home cage. 1 to 2 days post injection, the DRGs were collected as described above.

End-organ analyses

Glabrous skin analysis—For the Meissner corpuscle analysis between pedal pads and interpads in glabrous skin, P30 forepaw pedal pads and interpad tissue was isolated. This timepoint was chosen as Meissner corpuscles have developed at this age and can be readily identified based on the $S100^{+}$ lamellar core and NFH axons in dermal papillae. One out of every three consecutive sections was mounted on each slide to avoid counting the same corpuscle twice. The number of Meissner corpuscles divided by the epidermal area were plotted.

For the Meissner corpuscle analysis of the $Prx1^{Cre}; Lmx1b^{fl/fl}$ mutants and control littermates, the forepaws and hindpaw pedal pads of each animal were collected in the same OCT block for sectioning, tissue processing, and image analysis. One out of every three consecutive sections was mounted on each slide to avoid counting the same corpuscle twice. All sections, including those containing pad and those containing non-pad glabrous skin regions, were used for the analysis.

For the Meissner corpuscle analysis of the control and *Bmpr1a* cKO littermates, the forepaws of each animal were collected. For controls, mice from the following genotypes were pooled together for analysis; $Avil^{Cre/+}$, $Bmpr1a^{fl/fl}$, and $Bmpr1a^{fl/fl};Actvr1^{fl/+}$. For mutant mice, two $Avil^{Cre}; Bmpr1a^{fl/fl}; Acvr1^{fl/+}$ mice and one $Avil^{Cre}; Bmpr1a^{fl/fl}$ mouse were pooled for analysis. Fingertips and pedal pads were processed separately to examine whether any region-dependent changes exist. The tissues were cryosectioned and one out of three consecutive sections were mounted on each slide. Only sections containing pads or fingertips were used for the analysis.

For all conditions, tissue IHC stainings were done in parallel, with at least one control and one mutant processed together using the same reagents. DAPI was used to identify the dermal papillae structures inside which Meissner corpuscles are located. The number of dermal papillae was counted using the multipoint counting tool on FIJI. Neurofilament (NFH) and S100 were used to identify Meissner corpuscles. The polygon selection tool on FIJI was used to draw the outline of the $S100^{+}$ corpuscle located inside the dermal papillae,

and the “Measure” plugin was used to calculate its area. For the Meissner corpuscle density measurements, the ratio of the number of MCs over the number of dermal papillae was calculated. For the Meissner corpuscle area quantifications at each skin section, the sum of the $S100^+$ area was divided by the number of Meissner corpuscles, and the ratio was reported.

For the $S100^+$ nuclei measurements, pedal pad glabrous skin cryosections (5 to 15 per animal) were used for IHC. The sections were stained with NFH, S100 and DAPI. The DAPI and S100 co-localization were used to quantify the number of $S100^+$ cells inside dermal papillae and lamellar core.

Hairy skin analysis—Back hairy and paw hairy skin were collected, and the fat tissue was removed using a spatula. The skin was cut in small pieces and was processed according to the wholemount protocol with NFH, S100, and Troma antibodies. Control and mutant mice were processed in parallel. Troma was used to identify guard from non-guard hair follicles. For the hairy skin analysis of the control and *Bmpr1a* cKO littermates, for controls, mice from the following genotypes were pooled together for analysis; $Avil^{Cre/+}$, $Bmpr1a^{fl/fl}$ and $Bmpr1a^{fl/fl}$;$Actvr1^{fl/+}$. For mutant mice, two $Avil^{Cre}$; $Bmpr1a^{fl/fl}$; $Acvr1^{fl/+}$ mouse and one $Avil^{Cre}$; $Bmpr1a^{fl/fl}$ mouse were pooled for analysis. For the non-guard hair follicles, the $S100^+$ area of lanceolate endings was quantified using the polygon tool and reported for every hair follicle. The terminal Schwann cell number (TSCs) was quantified using the S100 and DAPI overlap at the base of the lanceolate endings.

For the skin IHC and RNAscope analysis, the tissues were imaged on a Zeiss LSM 700 confocal microscope using a 20x or 40x oil-immersion lens. Alkaline phosphatase-stained paws were imaged in a Zeiss AxioZoom microscope. For DRG image collection, a Zeiss brightfield microscope was used.

Single-cell collection, sequencing, and analysis

Dorsal root ganglia dissociation for cell picking—P5–P6 mice injected at P3–P4 with CTB^{555} on glabrous skin and CTB^{488} on hairy paw skin, as described above, were anesthetized on ice and then sacrificed. The tissues were dissected until the spinal column was reached and transferred on a plate with DMEM: F12 medium (DMEM: F12 1:1, prepared with 1% pen/strep and 2.5mM D-Glucose) on ice. The DRGs from cervical regions C5–C8 were dissected, and the roots were trimmed. DRGs of 1–3 mice were combined together and placed in an Eppendorf tube with DMEM: F12 medium on ice. Both male and female mice were used for the experiments. Then, DRGs were incubated for 13 min at 37°C in the following solution: 40 units papain, 4mg/ml Collagenase, 10mg/mL BSA, 1mg/mL hyaluronidase, 0.6mg/mL DNAse diluted in DMEM: F12 medium. The digestion was stopped with a stop solution consisting of 20mg/mL ovomucoid (trypsin inhibitor) and 20mg/mL BSA in DMEM: F12 medium. The DRGs were then triturated using fire-polished glass pipettes, and the dissociated neurons were filtered through a 70μm filter. The filtered cell mixture was placed in an Eppendorf tube on ice and immediately used for cell picking.

Single-cell isolation—The cell-isolation step was completed within 2–3 hours of DRG collection to minimize cell death. Drops of ~10μl of the cell mixture were placed on a

slide and inspected with an inverted fluorescent microscope. CTB^{488} and CTB^{555} positive cells with large diameters (~50–70μm) were identified, and a small (~1μl) amount of the cell solution was aspirated using a fire-polished ~80–100μm micropipette (Drummond #50002005) connected to an aspirator tube (Sigma #A5177). The cell mixture was washed with 1xPBS 1–2 times until isolated single cells were visible under the bright field view in a Zeiss AxioZoom microscope. The fluorescently positive cell of interest was then picked using a new glass micropipette and transferred to lysis buffer in a PCR tube. When a PCR tube strip (8 tubes) was filled, the cells were frozen at −80°C. The process was repeated with a new round of picking. In total, 15 mice were used for experiments yielding 150 cells. All cells from all picking cycles were stored at −80°C until cDNA synthesis.

cDNA synthesis, amplification, library preparation & sequencing—cDNA synthesis was performed using the SMART-Seq® v4 Ultra® Low Input RNA Kit for Sequencing (Takara #634894) according to kit instructions. We used 18 amplification cycles, and the cells were split up in 5 cDNA synthesis batches with 16–36 cells per round. cDNA was purified after amplification using Agencourt AMPure XP beads (Beckman Coulter #A63880). The DNA libraries were prepared using the Nextera XT DNA Library Preparation Kit (Illumina # FC-131–1024). The concentration and quality of cDNA were examined by Bioanalyzer (DFCI Molecular Biology Core). Sequencing was carried out in the Harvard Biopolymers Core using a NextSeq Mid 2 × 75 per flow cell run and paired-end reads.

Sequencing files processing and QC—Reads from the SMART-seq analysis were processed to counts through the bcbio RNA-seq pipeline implemented in the bcbio-nextgen project (https://bcbio-nextgen.readthedocs.org/en/latest/). Raw reads were examined for quality issues using FastQC http://www.bioinformatics.babraham.ac.uk/projects/fastqc/) to ensure library generation and sequencing were suitable for further analysis.

If necessary, adapter sequences, other contaminant sequences such as polyA tails, and low-quality sequences with PHRED quality scores less than five were trimmed from reads using atropos [https://github.com/jdidion/atropos; 10.5281/zenodo.596588]. Trimmed reads were aligned to UCSC build mm10 of the mus musculus genome (mouse) using STAR.[55] Alignments were checked for evenness of coverage, rRNA content, genomic context of alignments (for example, alignments in known transcripts and introns), complexity and other quality checks using a combination of FastQC, Qualimap[56], MultiQC (https://github.com/ewels/MultiQC) and custom tools.

Counts of reads aligning to known genes were generated by featureCounts.[57] In parallel, Transcripts Per Million (TPM) measurements per isoform were generated by quasialignment using Salmon.[58]

Cells from the SMART-seq analysis were filtered based on QC metrics: mapping rate >0.8, genes detected >10,000, exonic mapping rate >0.7, intronic mapping rate <0.25, rRNA mapping rate <0.1, mitochondrial gene mapping rate <0.1 and total reads > $1E10^6$. 142 cells were selected from the initial 150.

Cluster analysis and cell inclusion criteria—The Seurat (v4.3) package was used for clustering analysis (https://satijalab.org/seurat/). Data were normalized and scaled using the functions NormalizeData and ScaleData with default values. FindVariableFeatures was used with 2000 variable features and vst as selection method. 20 PCs were used for FindNeighbors and UMAP generation. The resolution used for finding clusters was 1.4.

Integration analysis—The SmartSeq and the Sharma *et al.* droplet-based datasets were combined and integrated using Seurat's SCTransform,[59] with 3000 features selected. 30 PCs were used for UMAP generation with 0.2 resolution.

Differential gene expression analysis—Differential expression (DE) analysis between hairy and glabrous samples in cluster 1 was performed using a pseudobulk approach, using DESeq2.[60] Counts were aggregated into "pseudo-samples" based on the day of collection and sample type (hairy/glabrous). This approach yielded 48 differentially expressed genes (adjusted p-value < 0.05) (Supplemental Table).

Schematics—The schematics in Figure 2D, S6A and S4A were created using BioRender.com.

Quantification and statistical analysis—All data are expressed as the mean +/− standard error of the mean (SEM). The number of animals per group, statistical methods, and p values used in each experiment are denoted in the figure legend. Comparisons between two groups in all experiments were performed using non-parametric tests (Mann Whitney Wilcoxon test). All p values are reported in the figure legend. One-way ANOVA or Kruskal Wallis test was used in the case of three or more groups of the same condition were compared. For ANOVA tests, post hoc comparisons were performed using the post hoc test indicated in the figure legend. The p values of post hoc comparisons are denoted in the legends. Unless otherwise noted, *, $p < 0.05$, **, $p<0.01$, ***, $p<0.001$. All statistics were performed using GraphPad Prism software.

Supplementary Material

Refer to Web version on PubMed Central for supplementary material.

Acknowledgments

We thank Lisa Goodrich, Shan Meltzer, Andrew Shuster, Jing Peng, Karina Lezgiyeva, Erica Huey, Annie Handler, Rosa Martinez-Garcia, Aniqa Tasnim, and Lijun Qi for comments on the manuscript; Shan Meltzer, Lijun Qi and Michael Iskols for sharing tissues and help with analysis; Randy Johnson and Jessica Lehoczky for sharing *Lmx1b*^{fl} mice; and Paul Yu for sharing *Bmpr1a*^{fl}*; Acvr1*^{fl} mice. We thank Yin Liu for feedback on the single cell isolation experiments and on RNAscope modifications in CTB$^{488/555}$ labeled DRGs; the Biopolymers Facility (Harvard) and HSPH Bioinformatics Core for help with sequencing and analysis; and the Molecular Biology Core Facilities at the Dana-Farber Cancer Institute for performing the Bioanalyzer testing. This work was supported by a Boehringer Ingelheim Fonds fellowship (CK), an Onassis Scholarship (CK), the Harvard Medical School Foundry Program (VB and JH), NIH R35 5R35NS097344-05 (D.D.G.), and the Edward R. and Anne G. Lefler Center for Neurodegenerative Disorders (D.D.G.). D.D.G. is an investigator of the Howard Hughes Medical Institute.

Data and code availability

All data reported in this study will be shared by the lead contact upon request.

References

1. Abraira VE, and Ginty DD (2013). The Sensory Neurons of Touch. Neuron 79, 618–639. 10.1016/j.neuron.2013.07.051. [PubMed: 23972592]
2. Handler A, and Ginty DD (2021). The Mechanosensory Neurons of Touch and their Mechanisms of Activation. Nat Rev Neurosci 22, 521–537. 10.1038/s41583-021-00489-x. [PubMed: 34312536]
3. McCray BA, and Scherer SS (2021). Axonal Charcot-Marie-Tooth Disease: from Common Pathogenic Mechanisms to Emerging Treatment Opportunities. Neurotherapeutics 18, 2269–2285. 10.1007/s13311-021-01099-2. [PubMed: 34606075]
4. Orefice LL, Mosko JR, Morency DT, Wells MF, Tasnim A, Mozeika SM, Ye M, Chirila AM, Emanuel AJ, Rankin G, et al. (2019). Targeting Peripheral Somatosensory Neurons to Improve Tactile-Related Phenotypes in ASD Models. Cell 178, 867–886.e24. 10.1016/j.cell.2019.07.024. [PubMed: 31398341]
5. Richards N, and McMahon SB (2013). Targeting novel peripheral mediators for the treatment of chronic pain. Br J Anaesth 111, 46–51. 10.1093/bja/aet216. [PubMed: 23794644]
6. Middleton SJ, Perez-Sanchez J, and Dawes JM (2022). The structure of sensory afferent compartments in health and disease. J Anat 241, 1186–1210. 10.1111/joa.13544. [PubMed: 34528255]
7. Meltzer S, Santiago C, Sharma N, and Ginty DD (2021). The cellular and molecular basis of somatosensory neuron development. Neuron 109, 3736–3757. 10.1016/j.neuron.2021.09.004. [PubMed: 34592169]
8. Lehnert BP, Santiago C, Huey EL, Emanuel AJ, Renauld S, Africawala N, Alkislar I, Zheng Y, Bai L, Koutsioumpa C, et al. (2021). Mechanoreceptor synapses in the brainstem shape the central representation of touch. Cell 184, 5608–5621.e18. 10.1016/j.cell.2021.09.023. [PubMed: 34637701]
9. Halata Z (1993). Sensory innervation of the hairy skin (light-and electronmicroscopic study). Journal of Investigative Dermatology 101, S75–S81. 10.1016/0022-202X(93)90505-C.
10. Horch KW, Tuckett RP, and Burgess PR (1977). A key to the classification of cutaneous mechanoreceptors. J Invest Dermatol 69, 75–82. 10.1111/1523-1747.ep12497887. [PubMed: 874346]
11. Burgess PR, Petit D, and Warren RM (1968). Receptor types in cat hairy skin supplied by myelinated fibers. Journal of Neurophysiology 31, 833–848. 10.1152/jn.1968.31.6.833. [PubMed: 5710537]
12. Suazo I, Vega JA, García-Mesa Y, García-Piqueras J, García-Suárez O, and Cobo T (2022). The Lamellar Cells of Vertebrate Meissner and Pacinian Corpuscles: Development, Characterization, and Functions. Frontiers in Neuroscience 16.
13. Olson W, Dong P, Fleming M, and Luo W (2016). The specification and wiring of mammalian cutaneous low-threshold mechanoreceptors. Wiley Interdiscip Rev Dev Biol 5, 389–404. 10.1002/wdev.229. [PubMed: 26992078]
14. Koltzenburg M, Stucky CL, and Lewin GR (1997). Receptive properties of mouse sensory neurons innervating hairy skin. J Neurophysiol 78, 1841–1850. 10.1152/jn.1997.78.4.1841. [PubMed: 9325353]
15. Walcher J, Ojeda-Alonso J, Haseleu J, Oosthuizen MK, Rowe AH, Bennett NC, and Lewin GR (2018). Specialized mechanoreceptor systems in rodent glabrous skin. J Physiol 596, 4995–5016. 10.1113/JP276608. [PubMed: 30132906]
16. Meltzer S, Boulanger KC, Osei-Asante E, Handler A, Zhang Q, Sano C, Itohara S, and Ginty DD (2022). A role for axon–glial interactions and Netrin-G1 signaling in the formation of low-threshold mechanoreceptor end organs. Proceedings of the National Academy of Sciences 119, e2210421119. 10.1073/pnas.2210421119.

17. Rutlin M, Ho C-Y, Abraira VE, Cassidy C, Bai L, Woodbury CJ, and Ginty DD (2014). The Cellular and Molecular Basis of Direction Selectivity of Aδ-LTMRs. Cell 159, 1640–1651. 10.1016/j.cell.2014.11.038. [PubMed: 25525881]

18. Neubarth NL, Emanuel AJ, Liu Y, Springel MW, Handler A, Zhang Q, Lehnert BP, Guo C, Orefice LL, Abdelaziz A, et al. (2020). Meissner corpuscles and their spatially intermingled afferents underlie gentle touch perception. Science 368, eabb2751. 10.1126/science.abb2751. [PubMed: 32554568]

19. Luo W, Enomoto H, Rice FL, Milbrandt J, and Ginty DD (2009). Molecular identification of rapidly adapting mechanoreceptors and their developmental dependence on ret signaling. Neuron 64, 841–856. 10.1016/j.neuron.2009.11.003. [PubMed: 20064391]

20. Idé C (1976). The fine structure of the digital corpuscle of the mouse toe pad, with special reference to nerve fibers. Am J Anat 147, 329–355. 10.1002/aja.1001470307. [PubMed: 983972]

21. Emanuel AJ, Lehnert BP, Panzeri S, Harvey CD, and Ginty DD (2021). Cortical Responses to Touch Reflect Subcortical Integration of LTMR Signals. Nature 600, 680–685. 10.1038/s41586-021-04094-x. [PubMed: 34789880]

22. Li L, Rutlin M, Abraira VE, Cassidy C, Kus L, Gong S, Jankowski MP, Luo W, Heintz N, Koerber HR, et al. (2011). The Functional Organization of Cutaneous Low-Threshold Mechanosensory Neurons. Cell 147, 1615–1627. 10.1016/j.cell.2011.11.027. [PubMed: 22196735]

23. Li L, and Ginty DD (2014). The structure and organization of lanceolate mechanosensory complexes at mouse hair follicles. Elife 3, e01901. 10.7554/eLife.01901. [PubMed: 24569481]

24. Lu CP, Polak L, Keyes BE, and Fuchs E (2016). Spatiotemporal antagonism in mesenchymal-epithelial signaling in sweat versus hair fate decision. Science 354, aah6102. 10.1126/science.aah6102. [PubMed: 28008008]

25. Badea TC, Cahill H, Ecker J, Hattar S, and Nathans J (2009). Distinct roles of transcription factors Brn3a and Brn3b in controlling the development, morphology, and function of retinal ganglion cells. Neuron 61, 852–864. 10.1016/j.neuron.2009.01.020. [PubMed: 19323995]

26. Usoskin D, Furlan A, Islam S, Abdo H, Lönnerberg P, Lou D, Hjerling-Leffler J, Haeggström J, Kharchenko O, Kharchenko PV, et al. (2015). Unbiased classification of sensory neuron types by large-scale single-cell RNA sequencing. Nat Neurosci 18, 145–153. 10.1038/nn.3881. [PubMed: 25420068]

27. Sharma N, Flaherty K, Lezgiyeva K, Wagner DE, Klein AM, and Ginty DD (2020). The emergence of transcriptional identity in somatosensory neurons. Nature 577, 392–398. 10.1038/s41586-019-1900-1. [PubMed: 31915380]

28. Zheng Y, Liu P, Bai L, Trimmer JS, Bean BP, and Ginty DD (2019). Deep Sequencing of Somatosensory Neurons Reveals Molecular Determinants of Intrinsic Physiological Properties. Neuron 103, 598–616.e7. 10.1016/j.neuron.2019.05.039. [PubMed: 31248728]

29. Stuart T, Butler A, Hoffman P, Hafemeister C, Papalexi E, Mauck WM, Hao Y, Stoeckius M, Smibert P, and Satija R (2019). Comprehensive Integration of Single-Cell Data. Cell 177, 1888–1902.e21. 10.1016/j.cell.2019.05.031. [PubMed: 31178118]

30. Li Y, Qiu Q, Watson SS, Schweitzer R, and Johnson RL (2010). Uncoupling skeletal and connective tissue patterning: conditional deletion in cartilage progenitors reveals cell-autonomous requirements for Lmx1b in dorsal-ventral limb patterning. Development 137, 1181–1188. 10.1242/dev.045237. [PubMed: 20215352]

31. Logan M, Martin JF, Nagy A, Lobe C, Olson EN, and Tabin CJ (2002). Expression of Cre Recombinase in the developing mouse limb bud driven by a Prxl enhancer. Genesis 33, 77–80. 10.1002/gene.10092. [PubMed: 12112875]

32. Abraira VE, Kuehn ED, Chirila AM, Springel MW, Toliver AA, Zimmerman AL, Orefice LL, Boyle KA, Bai L, Song BJ, et al. (2017). The Cellular and Synaptic Architecture of the Mechanosensory Dorsal Horn. Cell 168, 295–310.e19. 10.1016/j.cell.2016.12.010. [PubMed: 28041852]

33. Zhang Y, and Que J (2020). BMP Signaling in Development, Stem Cells, and Diseases of the Gastrointestinal Tract. Annual Review of Physiology 82, 251–273.

34. Glover JD, Sudderick ZR, Shih BB-J, Batho-Samblas C, Charlton L, Krause AL, Anderson C, Riddell J, Balic A, Li J, et al. (2023). The developmental basis of fingerprint pattern formation and variation. Cell 0. 10.1016/j.cell.2023.01.015.
35. Winnier G, Blessing M, Labosky PA, and Hogan BL (1995). Bone morphogenetic protein-4 is required for mesoderm formation and patterning in the mouse. Genes Dev. 9, 2105–2116. 10.1101/gad.9.17.2105. [PubMed: 7657163]
36. Lyons KM, Pelton RW, and Hogan BL (1989). Patterns of expression of murine Vgr-1 and BMP-2a RNA suggest that transforming growth factor-beta-like genes coordinately regulate aspects of embryonic development. Genes Dev 3, 1657–1668. 10.1101/gad.3.11.1657. [PubMed: 2481605]
37. Lyons KM, Pelton RW, and Hogan BL (1990). Organogenesis and pattern formation in the mouse: RNA distribution patterns suggest a role for bone morphogenetic protein-2A (BMP-2A). Development 109, 833–844. 10.1242/dev.109.4.833. [PubMed: 2226202]
38. Finelli MJ, Murphy KJ, Chen L, and Zou H (2013). Differential Phosphorylation of Smad1 Integrates BMP and Neurotrophin Pathways through Erk/Dusp in Axon Development. Cell Reports 3, 1592–1606. 10.1016/j.celrep.2013.04.011. [PubMed: 23665221]
39. Hasegawa H, Abbott S, Han B-X, Qi Y, and Wang F (2007). Analyzing Somatosensory Axon Projections with the Sensory Neuron-Specific Advillin Gene. J. Neurosci 27, 14404–14414. 10.1523/JNEUROSCI.4908-07.2007. [PubMed: 18160648]
40. Renehan WE, and Munger BL (1990). The development of meissner corpuscles in primate digital skin. Developmental Brain Research 51, 35–44. 10.1016/0165-3806(90)90256-X. [PubMed: 2297894]
41. Idé C (1977). Development of meissner corpuscle of mouse toe pad. The Anatomical Record 188, 49–67. 10.1002/ar.1091880107. [PubMed: 869232]
42. Livesey FJ, and Cepko CL (2001). Vertebrate neural cell-fate determination: Lessons from the retina. Nat Rev Neurosci 2, 109–118. 10.1038/35053522. [PubMed: 11252990]
43. Shrestha BR, Chia C, Wu L, Kujawa SG, Liberman MC, and Goodrich LV (2018). Sensory Neuron Diversity in the Inner Ear Is Shaped by Activity. Cell 174, 1229–1246.e17. 10.1016/j.cell.2018.07.007. [PubMed: 30078709]
44. Liu Y, Rutlin M, Huang S, Barrick CA, Wang F, Jones KR, Tessarollo L, and Ginty DD (2012). Sexually dimorphic BDNF signaling directs sensory innervation of the mammary gland. Science 338, 1357–1360. 10.1126/science.1228258. [PubMed: 23224557]
45. Jenkins BA, Fontecilla NM, Lu CP, Fuchs E, and Lumpkin EA (2019). The cellular basis of mechanosensory Merkel-cell innervation during development. eLife 8, e42633. 10.7554/eLife.42633. [PubMed: 30794158]
46. Guha U, Gomes WA, Samanta J, Gupta M, Rice FL, and Kessler JA (2004). Target-derived BMP signaling limits sensory neuron number and the extent of peripheral innervation in vivo. Development 131, 1175–1186. 10.1242/dev.01013. [PubMed: 14973275]
47. Hodge LK, Klassen MP, Han B-X, Yiu G, Hurrell J, Howell A, Rousseau G, Lemaigre F, Tessier-Lavigne M, and Wang F (2007). Retrograde BMP Signaling Regulates Trigeminal Sensory Neuron Identities and the Formation of Precise Face Maps. Neuron 55, 572–586. 10.1016/j.neuron.2007.07.010. [PubMed: 17698011]
48. Ji S-J, and Jaffrey SR (2012). Intra-axonal Translation of SMAD1/5/8 Mediates Retrograde Regulation of Trigeminal Ganglia Subtype Specification. Neuron 74, 95–107. 10.1016/j.neuron.2012.02.022. [PubMed: 22500633]
49. Iwasato T, and Erzurumlu RS (2018). Development of tactile sensory circuits in the CNS. Curr Opin Neurobiol 53, 66–75. 10.1016/j.conb.2018.06.001. [PubMed: 29908482]
50. Zhong J, and Zou H (2014). BMP signaling in axon regeneration. Current Opinion in Neurobiology 27, 127–134. 10.1016/j.conb.2014.03.009. [PubMed: 24713578]
51. Choi S, Hachisuka J, Brett MA, Magee AR, Omori Y, Iqbal N-A, Zhang D, DeLisle MM, Wolfson RL, Bai L, et al. (2020). Parallel ascending spinal pathways for affective touch and pain. Nature 587, 258–263. 10.1038/s41586-020-2860-1. [PubMed: 33116307]
52. Zhao Z-Q, Scott M, Chiechio S, Wang J-S, Renner KJ, Gereau RW, Johnson RL, Deneris ES, and Chen Z-F (2006). Lmx1b is required for maintenance of central serotonergic neurons and

mice lacking central serotonergic system exhibit normal locomotor activity. J Neurosci 26, 12781–12788. 10.1523/JNEUROSCI.4143-06.2006. [PubMed: 17151281]

53. Generation of Bmpr/Alk3 conditional knockout mice - Mishina - 2002 - genesis - Wiley Online Library https://onlinelibrary.wiley.com/doi/10.1002/gene.10038.
54. Gu Z, Reynolds EM, Song J, Lei H, Feijen A, Yu L, He W, MacLaughlin DT, van den Eijnden-van Raaij J, Donahoe PK, et al. (1999). The type I serine/threonine kinase receptor ActRIA (ALK2) is required for gastrulation of the mouse embryo. Development 126, 2551–2561. 10.1242/dev.126.11.2551. [PubMed: 10226013]
55. Dobin A, Davis CA, Schlesinger F, Drenkow J, Zaleski C, Jha S, Batut P, Chaisson M, and Gingeras TR (2013). STAR: ultrafast universal RNA-seq aligner. Bioinformatics 29, 15–21. 10.1093/bioinformatics/bts635. [PubMed: 23104886]
56. García-Alcalde F, Okonechnikov K, Carbonell J, Cruz LM, Götz S, Tarazona S, Dopazo J, Meyer TF, and Conesa A (2012). Qualimap: evaluating next-generation sequencing alignment data. Bioinformatics 28, 2678–2679. 10.1093/bioinformatics/bts503. [PubMed: 22914218]
57. Liao Y, Smyth GK, and Shi W (2014). featureCounts: an efficient general purpose program for assigning sequence reads to genomic features. Bioinformatics 30, 923–930. 10.1093/bioinformatics/btt656. [PubMed: 24227677]
58. Patro R, Duggal G, Love MI, Irizarry RA, and Kingsford C (2016). Salmon provides accurate, fast, and bias-aware transcript expression estimates using dual-phase inference. 021592. 10.1101/021592.
59. Hafemeister C, and Satija R (2019). Normalization and variance stabilization of single-cell RNA-seq data using regularized negative binomial regression. Genome Biol 20, 296. 10.1186/s13059-019-1874-1. [PubMed: 31870423]
60. Love MI, Huber W, and Anders S (2014). Moderated estimation of fold change and dispersion for RNA-seq data with DESeq2. Genome Biol 15, 550. 10.1186/s13059-014-0550-8. [PubMed: 25516281]

Highlights

- Touch end-organ morphogenesis occurs postnatally and is instructed by the skin
- Neurons innervating both glabrous and hairy skin form skin type-appropriate endings
- *BMP5* and *BMP7* are enriched in glabrous skin at developmentally critical timepoints
- Formation of Meissner corpuscles is dependent on BMP receptor signaling

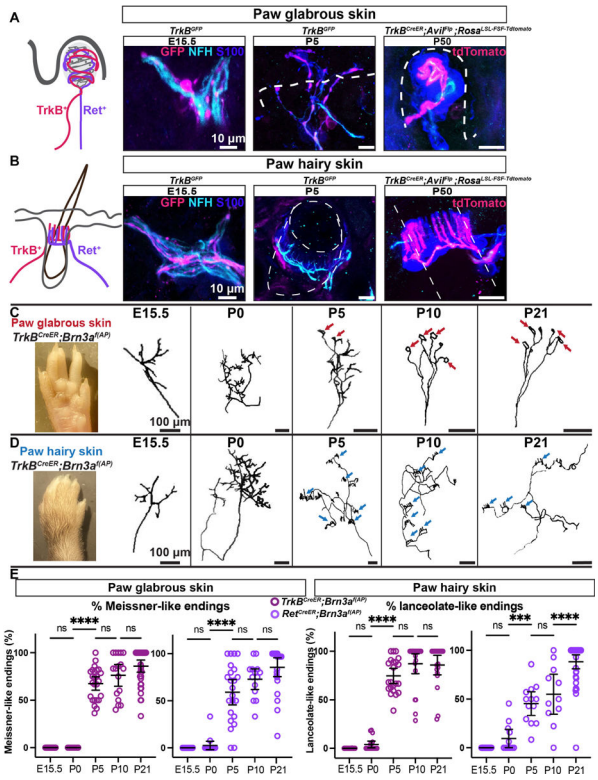

Figure 1. LTMR axon terminals in glabrous and hairy skin are comparable embryonically but diverge in the first postnatal week

(A and B) Example images of *TrkB*$^{+}$ endings (*TrkB*^{GFP} or *TrkB*^{CreER}; *Avil*^{Flp}; *Rosa*$^{LSL\text{-}FSF\text{-}Tdtomato}$) in paw glabrous skin (A) and paw hairy skin (B) at E15.5, P5, and P50. The sections were stained with S100, NFH and GFP or tdTomato. The white dotted lines represent the dermal-epidermal junction in glabrous skin and the hair follicle outline in hairy skin. TrkB^{+} and Ret^{+} endings in glabrous skin innervate Meissner corpuscles in dermal papillae. TrkB^{+} and Ret^{+} endings in hairy skin form longitudinal lanceolate endings around hair follicles (Ret^{+} endings are present around guard and awl/auchene hair follicles, while TrkB^{+} endings around awl/auchene and zigzag hair follicles).

(C and D) Example reconstructions of sparsely labeled *TrkB*^{CreER}; *Brn3a*$^{f(AP)}$ endings in paw glabrous skin (C) and paw hairy skin (D) at different developmental ages. Red arrows point to developing Meissner corpuscles while blue arrows to developing lanceolate endings.

(E) Quantification of percentages of Meissner-like endings (left panel) in paw glabrous skin of *TrkB*^{CreER}; *Brn3a*$^{f(AP)}$ and *Ret*^{CreER}; *Brn3a*$^{f(AP)}$ across development. Each datapoint represents the quantification of endings from a single neuron. Quantification of percentages of lanceolate-like endings (right panel) in paw hairy skin of *TrkB*^{CreER}; *Brn3a*$^{f(AP)}$ and *Ret*^{CreER}; *Brn3a*$^{f(AP)}$ sensory neurons across development (n=3–5 mice per timepoint and per genotype).

For Meissner ending analysis: *TrkB*^{CreER}; *Brn3a*$^{f(AP)}$ one-way-ANOVA $p<0.0001$, $R^2=0.8$, *Ret*^{CreER};*Brn3a*$^{f(AP)}$ one-way-ANOVA $p<0.0001$, $R^2=0.7$.

Pairwise comparisons for *TrkB*^{CreER}; *Brn3a*$^{f(AP)}$ were performed: E15.5 vs P0 $p>0.99$, P0 vs P5 $p<0.0001$, P5 vs P10 $p=0.43$ and P10 vs P21 $p=0.25$.

Pairwise comparisons for *Ret*^{CreER}*; Brn3a*$^{f(AP)}$ were performed: E15.5 vs P0 p=0.99, P0 vs P5 p<0.0001, P5 vs P10 p=0.29 and P10 vs P21 p=0.37.
For lanceolate-ending analysis: *TrkB*^{CreER}*; Brn3a*$^{f(AP)}$ one-way-ANOVA p<0.0001, R^2=0.86, *Ret*^{CreER}*;Brn3a*$^{f(AP)}$ one-way-ANOVA p<0.0001, R^2=0.79.
Pairwise comparisons for *TrkB*^{CreER}*; Brn3a*$^{f(AP)}$ were performed: E15.5 vs P0 p=0.93, P0 vs P5 p<0.0001, P5 vs P10 p=0.09 and P10 vs P21 p=0.99.
Pairwise comparisons for *Ret*^{CreER}*; Brn3a*$^{f(AP)}$ were performed: E15.5 vs P0 p= 0.65, P0 vs P5 p=0.0001, P5 vs P10 p=0.73 and P10 vs P21 p<0.0001.
See also Figure S1, S2.

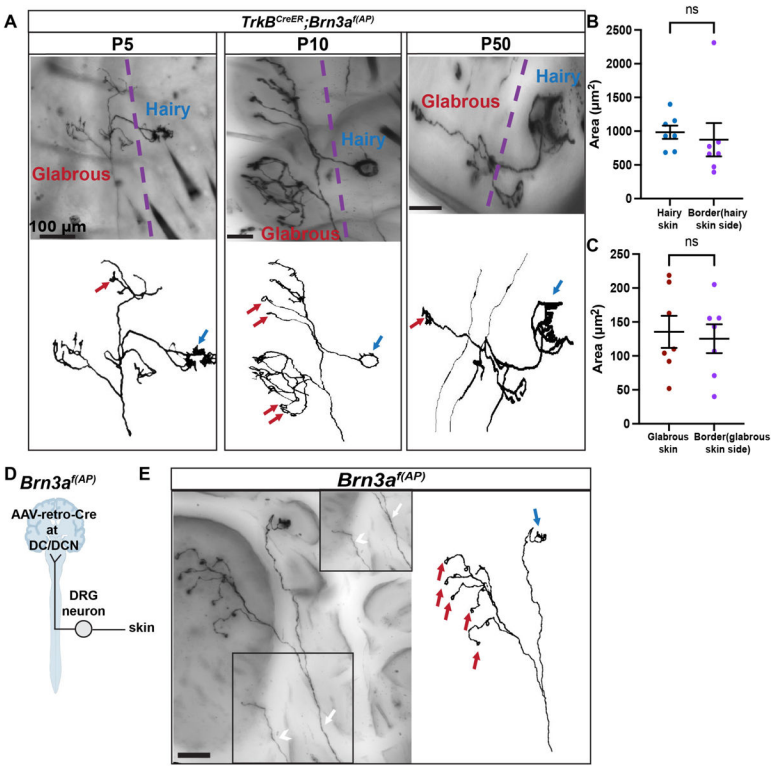

Figure 2. Individual neurons with branches that extend into both glabrous and hairy skin form ending types appropriate for both skin regions

(A) Representative example images (top) and reconstructions (bottom) of P5, P10 and P50 "border neurons" from *TrkB*^{CreER}*; Brn3a*$^{f(AP)}$ mice. These neurons terminate in the finger of the paws and exhibit branches that form both lanceolate endings in hairy skin (blue arrows) and Meissner corpuscle endings in glabrous skin (red arrows). The purple dotted line indicates the approximate border of glabrous and hairy skin.

(B) End-organ area quantifications from *TrkB*^{CreER}*; Brn3a*$^{f(AP)}$ endings terminating in hairy paw skin. Lanceolate endings that terminate only in hairy skin and endings from border neuron branches in hairy skin have similar areas. Each datapoint represents the area of a single lanceolate ending. N=3 mice per group. Mann Whitney test p=0.09, U=11.

(C) End-organ area quantifications from *TrkB*^{CreER}*; Brn3a*$^{f(AP)}$ Meissner corpuscle endings terminating only in paw glabrous skin and endings from border neuron branches in glabrous skin. Each datapoint represents a single Meissner corpuscle. N=3 mice per group. Mann Whitney test p=0.7, U=21.

(D) Schematic of brainstem viral labeling approach. AAV-retro-Cre virus was injected in the dorsal column (DC) or dorsal column nuclei (DCN) of *Brn3a*$^{f(AP)}$ mice.

(E) Representative example image (left) and reconstruction (right) of an identified border neuron. The neuron terminates in the ventral hindpaw innervating the hair follicles (blue arrows) present in the middle of the paw on one side and the glabrous pedal pads on the other (red arrows). The imaging approach distinguishes single axons, the white arrow indicates the border neuron axon in the skin while the white arrowhead points to a neighboring axon, also shown in the inset (top right corner).

See also Figure S3 and Supplementary Videos 1–3.

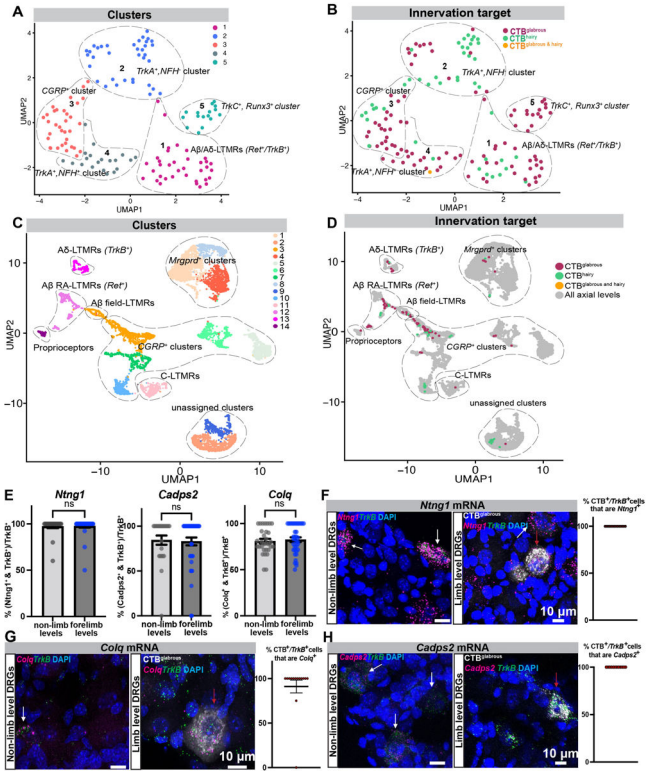

Figure 3. Transcriptional signatures of glabrous and hairy skin innervating neuronal classes

(A) UMAP plot with the clusters identified from the P5 sensory neuron cell picking experiment: cluster 1, 36 neurons (10 hairy skin innervating, 26 glabrous skin innervating neurons); cluster 2, 36 neurons (22 hairy skin innervating, 14 glabrous skin innervating); cluster 3, 34 neurons (10 hairy skin innervating, 24 glabrous skin innervating); cluster 4, 20 neurons (2 hairy skin innervating, 1 glabrous and hairy skin innervating, 17 glabrous skin innervating); and cluster 5, 16 neurons (16 glabrous skin innervating).

(B) UMAP plot with color-coding according to the innervation target (glabrous skin innervation, hairy skin innervation, or for one neuron both glabrous and hairy skin).

(C) UMAP plot and clusters of the integration analysis from the P5 cell picking and P5 scRNA seq dataset.

(D) UMAP plot of the integration analysis with color-coding according to the innervation target

(E) Quantification of the percentages of cells double-positive for *TrkB*$^{+}$ and *Ntng1/Cadps2/Colq* in nonlimb and forelimb (C5–C8) DRGs, n=3 mice per condition. All comparisons were done using the Mann Whitney test. For *Ntng1*: p>0.9, U=402, 35 C5–C8 and 23 non-limb cells quantified, *Cadps2*: p=0.98, U=447, 39 C5–C8 and 23 non-limb cells quantified, *Colq*: p =0.58, U=529 37 C5–C8 and 31 non-limb cells quantified.

(F) Example images (left panels) of RNAscope for *Ntng1* and *TrkB* mRNA. Nonlimb and limb level DRG sections of P5 mice injected with CTB in forepaw glabrous skin (CTB^{glabrous}) were examined. White arrows point to *Ntng1* and *TrkB* double positive and red arrows to CTB, *TrkB* and *Ntng1* triple positive cells. Quantifications (right panel) of the percentages of neurons that were triple positive for CTB, *TrkB* and *Ntng1* (14 cells analyzed from 3 mice).

(G) Example images (left panels) of RNAscope for *Colq* and *TrkB* mRNA. Nonlimb and limb level DRG sections of P5 mice injected with CTB into forepaw glabrous skin ($CTB^{glabrous}$) were examined. White arrows point to *TrkB* and *Colq* double positive and red arrows to CTB, *TrkB* and *Colq* triple positive cells. Quantifications (right panel) of the percentages of neurons that were triple positive for CTB, *TrkB* and *Colq* (14 cells analyzed from 3 mice).

(H) Example images (left panels) of RNAscope for *Cadps2* and *TrkB* mRNA. Nonlimb and limb level DRG sections of P5 mice injected with CTB in forepaw glabrous skin ($CTB^{glabrous}$) were examined. White arrows point to *TrkB* and *Cadps2* double positive and red arrows to CTB, *TrkB* and *Cadps2* triple positive cells. Quantifications (right panel) of the percentages of neurons that were triple positive for CTB, *TrkB* and *Cadps2* (12 cells analyzed from 3 mice).

See also Figure S4.

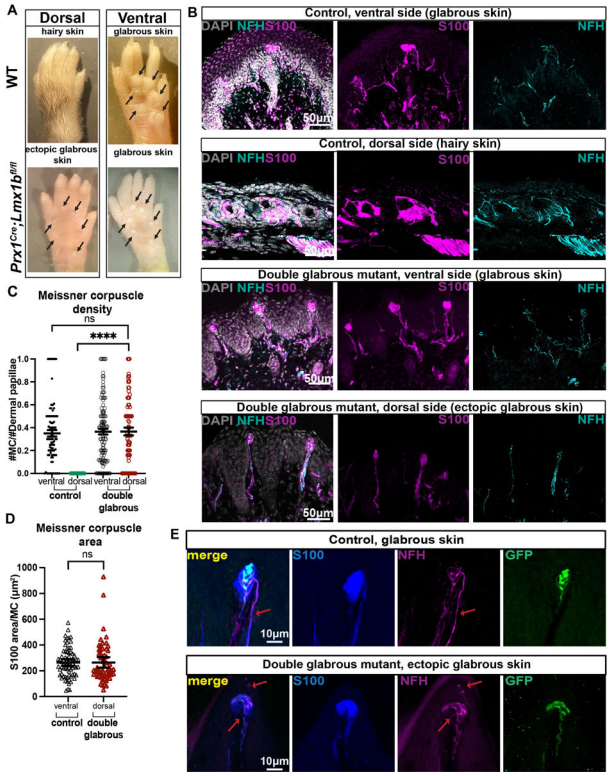

Figure 4. Ectopic glabrous skin in double glabrous mutant mice becomes innervated and displays Meissner corpuscle-like structures

(A) Example images of the dorsal and ventral surfaces of wild type and *Prx1*^{Cre}*; Lmx1b*$^{fl/fl}$ mice, also referred to as double glabrous mutants. The majority of the dorsal surface of the mutants is covered by glabrous skin, with areas of hairy skin interspersed. Black arrows point to the pedal pads. A small amount of hair removal (Nair) was applied to all surfaces.

(B) Sections of P21 control and double glabrous forepaws with NFH, S100, and DAPI. Control ventral and dorsal skin regions (top two rows) have Meissner corpuscles on the ventral side and lanceolate endings on the dorsal side. Double glabrous mutant ventral and dorsal skin (bottom two rows) is predominantly glabrous, and these mutants contain Meissner corpuscles on both the ventral and dorsal sides of the paw. Hair follicles innervated with lanceolate endings are found in some of the mutant's dorsal surfaces.

(C) Quantifications of Meissner corpuscles density (Meissner corpuscles divided by the number of dermal papillae) in control and double glabrous mice demonstrate that they are similar in control ventral, double glabrous dorsal, and double glabrous ventral skin but distinct from control dorsal skin. Each datapoint represents a forepaw/hindpaw skin section. N=3–4 mice were analyzed per genotype, 85 sections for control ventral, 19 for control dorsal, 127 for double glabrous ventral, and 78 for dorsal, One-way Kruskal Wallis test $p<0.0001$, Kruskal Wallis statistic 43.21. Additional Mann Whitney tests between two conditions: ns, and <0.0001, Mann Whitney U=209.

(D) Lamellar cell area of Meissner corpuscles quantified in skin sections of forepaw and hindpaw skin in control and double glabrous mice. Each datapoint represents the average $S100^{+}$ area of Meissner corpuscles in a skin section. N=3 mice per condition, 72 control and 59 double glabrous sections quantified (Mann Whitney test $p=0.4$, U=1951).

(E) Forelimb pedal pad sections of control *Npy2r-GFP* glabrous skin (top) and *Prx1*^{Cre}*; Lmx1b*$^{fl/fl}$*; Npy2r-GFP* double glabrous mutant, ectopic glabrous skin (bottom). The sections are stained using S100, GFP and NFH. Red arrows point to the GFP^{-} axon (presumably Ret^{+}). N=3 mice per condition.
See also Figure S5.

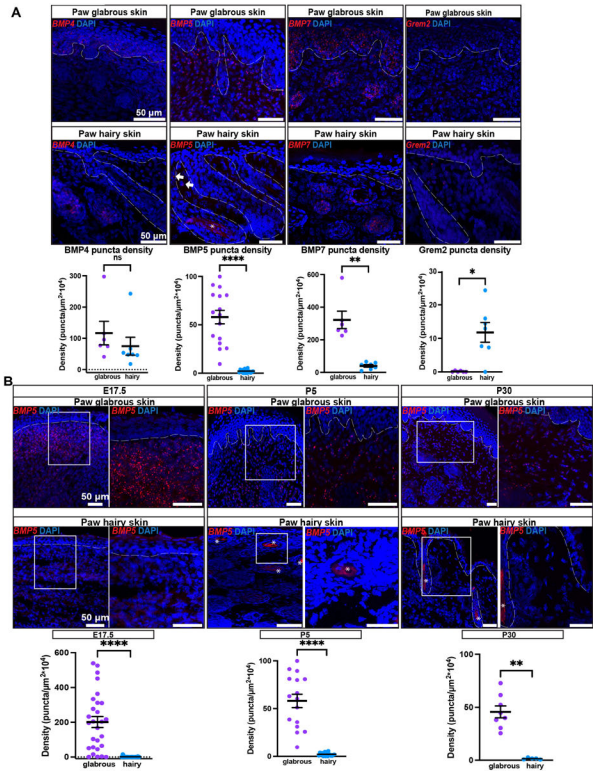

Figure 5. Characterization of BMP ligand expression patterns in paw glabrous and hairy skin over development

(A) Example forepaw glabrous and hairy skin images visualizing *BMP4, BMP5*, *BMP7* and *Grem2* puncta at P5 (top panels) and puncta density quantifications (bottom panels). The asterisk indicates background signal in the hair shaft, and the arrows point to the mRNA signal. The dotted lines outline the dermo-epidermal junction in all panels. N=3 mice per group. The puncta density of *BMP4, BMP5, BMP7* and *Grem2* at P5 control glabrous and hairy skin are shown in the bottom panels. Mann Whitney test from left to right: p=0.13, p<0.0001, p= 0.001 and p=0.01. N=3 mice per condition.

(B) *BMP5* mRNA in skin sections of forepaw glabrous skin and forepaw hairy skin (top panels) and puncta density quantifications (bottom panels). A lower (left panel) and higher magnification (right panel, outlined in a white rectangle) are presented. The skin was examined at E17.5, P5 and P30 using *in situ* RNAscope. *BMP5* puncta are enriched in the glabrous skin at all time points. The asterisk indicates background signal in the hair shaft. N=3 mice per group. The bottom panels include quantifications of *BMP5* puncta density at E17.5, P5 and P30 control glabrous and hairy skin. Mann Whitney test from left to right: p<0.0001, p<0.0001 and p=0.001. N=3 mice per condition.

See also Figure S6.

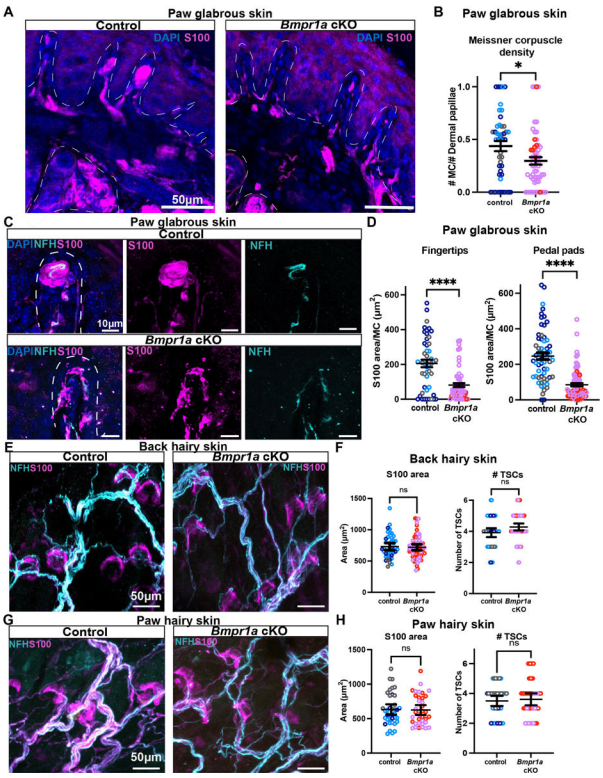

Figure 6. Conditional deletion of genes encoding BMP type I receptors in somatosensory neurons leads to dysmorphic Meissner corpuscles

(A) Sections of forepaw pedal pad glabrous skin of *Avil*^{Cre}*; Bmpr1a*$^{fl/fl}$ and control littermate P30 mice. The dotted lines outline the dermal-epidermal junction and sweat glands. S100 was used to investigate the presence of Meissner corpuscles and DAPI the overall skin composition.

(B) Quantifications of Meissner corpuscle density in forepaw fingertips in control and mutant mice (P28-P35). *Bmpr1a* cKO had comparable densities, which were decreased compared to control littermates. Each datapoint represents the Meissner corpuscle density quantified in a skin section; 46 control and 58 mutant sections. Mann Whitney test p=0.02, U=981. N=3 controls; *Avil*$^{Cre/+}$ (blue dots), *Bmpr1a*$^{fl/fl}$ (light blue dots), and *Bmpr1a*$^{fl/fl}$*;Actvr1*$^{fl/+}$ mice (grey dots). N=3 mutants; two *Avil*^{Cre}*; Bmpr1a*$^{fl/fl}$*; Acvr1*$^{fl/+}$ mice (pink dots) and one *Avil*^{Cre}*; Bmpr1a*$^{fl/fl}$ mouse (red dots). Mutant mice were born in sub-Mendelian ratios.

(C) Sections of forepaw pedal pad skin and example images of Meissner corpuscles in control and mutant mice. The dotted line outlines a dermal papilla. The sections were stained with S100 to visualize the lamellar cell core, NFH for the myelinated axons and DAPI.

(D) Quantifications of the lamellar S100^{+} area per Meissner corpuscle across forepaw fingertip (left panel) and forepaw pedal pads (right panel) in control and mutant mice. Each datapoint represents the S100^{+} area per MC quantified in a section of skin (for fingertips 49 control and 59 mutant sections, Mann Whitney test p<0.0001, U=799, for pedal pads 62 control and 80 mutant sections, Mann Whitney test p<0.0001, U=758.5). N=3 controls including *Avil*$^{Cre/+}$ (blue dots), *Bmpr1a*$^{fl/fl}$ (light blue dots), *Bmpr1a*$^{fl/fl}$*;Actvr1*$^{fl/+}$ mice

(grey dots), n=3 mutants including two *Avil*^{Cre}*; Bmpr1a*$^{fl/fl}$*; Acvr1*$^{fl/+}$mice (pink dots) and one *Avil*^{Cre}*; Bmpr1a*$^{fl/fl}$ mouse (red dots).

(E) Example images of back hairy skin wholemount staining of control and mutant mice. Overall innervation and lanceolate ending morphology are preserved in the mutants.

(F) Quantifications of the terminal Schwann cell number and S100 area of lanceolate endings in back hairy skin. Each datapoint represents the Schwann cell S100 area or number of TSCs, respectively, for every non-guard hair follicle ending quantified. The lanceolate ending S100^{+} area (left panel) was similar in control (endings in 44 hair follicles quantified) and mutant mice (endings in 62 hair follicles quantified) n= 3 controls, n= 3 mutants, (two *Avil*^{Cre}*;Bmpr1a*$^{fl/fl}$*;Acvr1*$^{fl/+}$ mice in pink, and one *Avil*^{Cre}*;Bmpr1a*$^{fl/fl}$ in red, which were combined for statistical analysis). The number of TSCs (right panel) was similar in control (endings in 48 hair follicles quantified) and mutant mice (endings in 65 hair follicles quantified) (Mann Whitney p=0.82, U=1329 and p =0.053, U=1245 respectively). Controls genotypes are: *Avil*$^{Cre/+}$ (blue dots), *Bmpr1a*$^{fl/fl}$ (light blue dots), and *Bmpr1a*$^{fl/fl}$*;Actvr1*$^{fl/+}$ (grey dots).

(G) Example images of paw hairy skin wholemount staining of control and mutant mice. Overall innervation and lanceolate ending morphology is preserved in the mutants.

(H) Similar analysis as in (F) in the forepaw hairy skin of control and mutant mice. The lanceolate ending S100^{+} area (left panel) was similar in control (endings in 38 hair follicles quantified) and mutant mice (endings in 37 hair follicles quantified). The number of TSCs (right panel) was similar in control (endings in 40 hair follicles quantified) and mutant mice (endings in 38 hair follicles quantified) (Mann Whitney p=0.76, U=674 and p=0.9, U=750.5 respectively). Control genotypes are *Avil*$^{Cre/+}$ (blue dots), *Bmpr1a*$^{fl/fl}$ (light blue dots), and *Bmpr1a*$^{fl/fl}$*;Actvr1*$^{fl/+}$ (grey dots).

See also Figure S7.

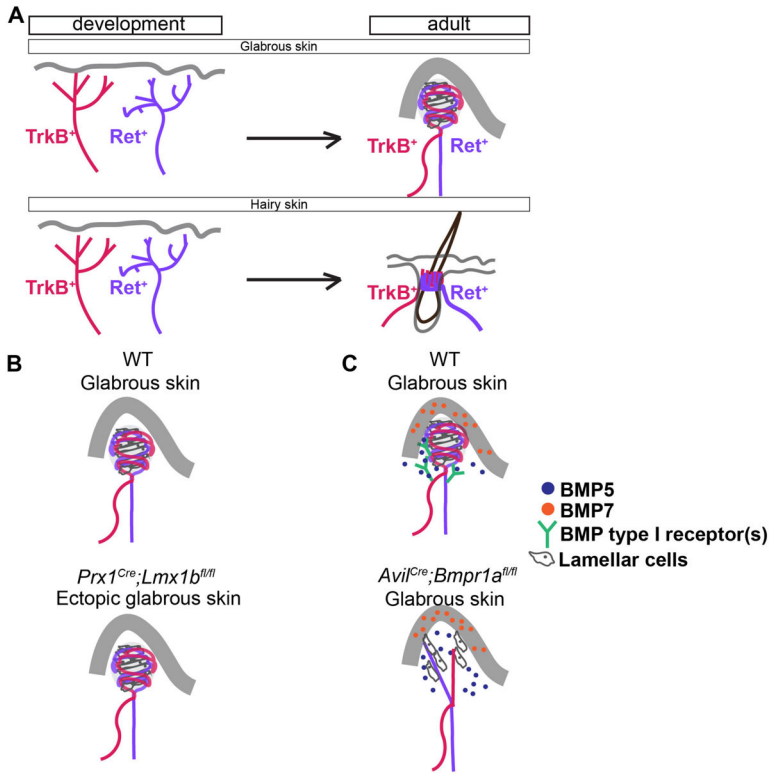

Figure 7. Model of LTMR development and its skin dependence

(A) Spatiotemporal development of TrkB$^+$ and Ret$^+$ Meissner corpuscle innervating and lanceolate ending forming neurons.

(B) Dorsal-ventral skin alterations lead to ectopic Meissner corpuscle development.

(C) *Bmpr1a* cKO mice exhibit highly aberrant Meissner development.

Key resources table

REAGENT or RESOURCE	SOURCE	IDENTIFIER
Antibodies		
rabbit polyclonal anti-S100 Beta	Fisher	15146-1-AP
chicken polyclonal anti-NFH	Aves labs	NFH0211
rabbit anti-NF200	Sigma	N4142
mouse monoclonal anti-NeuN	Millipore	AB_2298772
rat polyclonal anti-Troma1	DSHB	AB_531826
rabbit anti-DsRed	Clontech	AB_10013483
goat anti-GFP	Abcam	AB_305635
goat anti-mCherry	Cedarlane	AB0040-200
guinea pig anti-vGluT1	Millipore	AB_2301751
rabbit anti-Homer1	Synaptic Systems	160003
Isolectin B4 647	Invitrogen	SCR_014365
Alexa 546	Life Technologies	A11056
Alexa 488, 647	Jackson ImmunoResearch	706-605-148, 703-545-155
Bacterial and virus strains		
AAV2-retro-hSyn-Cre-WPRE	Addgene	105553-AAVrg
Chemicals, peptides, and recombinant proteins		
Tamoxifen	Sigma	T5648-1g
BCIP	Sigma	11383221001
NBT	Sigma	11383213001
Benzyl Alcohol	Sigma	402834
Benzyl Benzoate	Sigma	B-6630
Sunflower seed oil	Sigma	S5007
Paraformaldehyde, reagent grade, crystalline	Millipore Sigma	P6148-500G
10% Neutral buffered saline	Sigma	HT5012-1CS
Critical commercial assays		
SMART-Seq® v4 Ultra® Low Input RNA Kit for Sequencing	Takara	634894
RNAscope Fluorescent Multiplex Assay	ACD Bio	320850
RNAscope Protease III & Protease IV Reagents	ACD Bio	322340
RNAscope Probe Diluent	ACD Bio	300041
RNAscope Fluorescent Multiplex Assay v.2	ACD Bio	323110
RNAscope H2O2 & Protease Reagents	ACD Bio	322381
Opal 570	Akoya	FP1488001KT
Opal 690	Akoya	FP1497001KT
Opal 520	Akoya	FP1487001KT
Experimental models: Organisms/strains		
Mouse: *Avil*^{iCre}	Hasegawa et al.[39] and JAX	032536

REAGENT or RESOURCE	SOURCE	IDENTIFIER
Mouse: *Brn3a*$^{f(Ap)}$	Badea et al.[25] and JAX	010558
Mouse: *Rosa26*$^{FSF\text{-}LSL\text{-}tdTomato}$ (Ai65)	JAX	021875
Mouse: *Ret*^{CreER}	Luo et al., 2009 [19]	MGI 4437245
Mouse: *TrkB*^{CreER}	Rutlin et al., 2014[17] and JAX	027214
Mouse: *Advillin*^{Flp}	Choi et al., 2020[51]	n/a
Mouse: *TrkB*^{GFP}	Li L., et al.[22] and JAX	023046
Mouse: *Npy2r*^{GFP}	Li L., et al.	MGI 3844094
Mouse: *Prx1*^{Cre}	JAX	005584
Mouse: *Lmx1b*	Courtesy of Randy Johnson[52]via Jessica Lehoczky, now available at JAX	031287
Mouse: *Bmpr1a*^{fl}	Courtesy of Paul Yu[53]	n/a
Mouse: *Acvr1*^{fl}	Courtesy of Paul Yu[54]	n/a
Oligonucleotides		
Mm-Ntng1-C1	ACD Bio	488871
Mm-Ntng1-C2	ACD Bio	488871-C2
Mm-Cadps2-C2	ACD Bio	529361-C2
Mm-Ret-C3	ACD Bio	431791-C3
Mm-Ntrk2-C3	ACD Bio	423611-C3
Mm-Colq-C2	ACD Bio	496211-C2
Mm-Bmpr1a	ACD Bio	312421
Mm-Krt14	ACD Bio	422521
Mm-Bmp7	ACD Bio	407901
Mm-Bmp4-C3	ACD Bio	401301-C3
Mm-Grem1-C2	ACD Bio	314741-C2
Mm-Bmp5	ACD Bio	401241
Mm-BDNF	ACD Bio	424821
Software and algorithms		
ImageJ	NIH	https://imagej.nih.gov/ij/; RRID: SCR_003070
GraphPad Prism	GraphPad Software	https://www.graphpad.com/scientific-software/prism/
R studio version 2022.12.0+353	RStudio	https://posit.co/download/rstudio-desktop/
Seurat package	Satija Lab	https://satijalab.org/seurat/articles/install.html
Other		
NAIR hair removal cream	Church and Dwight Co.; Princeton, NJ	n/a
Fluoromount-G	Fisher	0100-20